Development of Korean Air Quality Prediction System version 1 (KAQPS v1) with focuses on practical issues

Kyunghwa Lee[1,2], Jinhyeok Yu[2], Sojin Lee[3], Mieun Park[4,5], Hun Hong[2], Soon Young Park[2], Myungje Choi[6], Jhoon Kim[6], Younha Kim[7], Jung-Hun Woo[7], Sang-Woo Kim[8] and Chul H. Song[2*]

1. Environmental Satellite Center, Climate and Air Quality Research Department, National Institute of Environmental Research (NIER), Incheon, Republic of Korea
2. School of Earth Sciences and Environmental Engineering, Gwangju Institute of Science and Technology (GIST), Gwangju, Republic of Korea
3. Department of Earth and Atmospheric Sciences, University of Houston, Texas, USA
4. Air Quality Forecasting Center, Climate and Air Quality Research Department, National Institute of Environmemnbntal Research (NIER), Incheon, Republic of Korea
5. Environmental Meteorology Research Division, National Institute of Meteorological Sciences (NIMS), Jeju, Republic of Korea
6. Department of Atmospheric Sciences, Yonsei University, Seoul, Republic of Korea
7. Department of Advanced Technology Fusion, Konkuk University, Seoul, Republic of Korea
8. School of Earth and Environmental Sciences, Seoul National University, Seoul, Republic of Korea

Short title: Air quality prediction system in Korea

Corresponding author: Chul H. Song (chsong@gist.ac.kr)

Abstract

For the purpose of providing reliable and robust air quality predictions, an air quality prediction system was developed for the main air quality criteria species in South Korea (PM_{10}, $PM_{2.5}$, CO, O_3, and SO_2). The main caveat of the system is to prepare the initial conditions (ICs) of the Community Multi-scale Air Quality (CMAQ) model simulations using observations from the Geostationary Ocean Color Imager (GOCI) and ground-based monitoring networks in northeast Asia. The performance of the air quality prediction system was evaluated during the Korea-United States Air Quality Study (KORUS-AQ) campaign period (1 May–12 June 2016). Data assimilation (DA) of optimal interpolation (OI) with Kalman filter was used in this study. One major advantage of the system is that it can predict not only particulate matter (PM) concentrations but also PM chemical composition including five main constituents: sulfate (SO_4^{2-}), nitrate (NO_3^-), ammonium (NH_4^+), organic aerosols (OAs), and elemental carbon (EC). In addition, it is also capable of predicting the concentrations of gaseous pollutants (CO, O_3 and SO_2). In this sense, this new air quality prediction system is comprehensive. The results with the ICs (DA RUN) were compared with those of the CMAQ simulations without ICs (BASE RUN). For almost all of the species, the application of ICs led to improved performance in terms of correlation, errors, and biases over the entire campaign period. The DA RUN agreed reasonably well with the observations for PM_{10} (IOA = 0.60; MB = -13.54) and $PM_{2.5}$ (IOA = 0.71; MB = -2.43) as compared to the BASE RUN for PM_{10} (IOA = 0.51; MB = -27.18) and $PM_{2.5}$ (IOA = 0.67; MB = -9.9). A significant improvement was also found with the DA RUN in terms of bias. For example, for CO, the MB of -0.27 (BASE RUN) was greatly enhanced to -0.036 (DA RUN). In the cases of O_3 and SO_2, the DA RUN also showed better performance than the BASE RUN. Further, several more practical issues frequently encountered in the air

quality prediction system were also discussed. In order to attain more accurate ozone predictions, the DA of NO_2 mixing ratios should be implemented with careful consideration of the measurement artifacts (i.e., inclusion of alkyl nitrates, HNO_3, and PANs in the ground-observed NO_2 mixing ratios). It was also discussed that, in order to ensure accurate nocturnal predictions of the concentrations of the ambient species, accurate predictions of the mixing layer heights (MLH) should be achieved from the meteorological modeling. Several advantages of the current air quality prediction system, such as its non-static free parameter scheme, dust episode prediction, and possible multiple implementations of DA prior to actual predictions, were also discussed. These configurations are all possible because the current DA system is not computationally expensive. In the ongoing and future works, more advanced DA techniques such as the three-dimensional variational (3DVAR) method and ensemble Kalman filter (EnK) are being tested and will be introduced to the Korean air quality prediction system (KAQPS).

Keywords: Air quality prediction; Particulate matter (PM); Geostationary satellite sensor (GOCI); Air Korea; Data assimilation (DA); Dust episode predictions; NO_2 measurement artifacts

1. Introduction

Air quality has long been considered an important issue in climate change, visibility, and public health, and it is strongly dependent upon meteorological conditions, emissions, and the transport of air pollutants. Air pollutants typically consist of atmospheric particles and gases such as particulate matter (PM), carbon monoxide (CO), ozone (O_3), nitrogen dioxide (NO_2), and sulfur dioxide (SO_2). These aerosols and gases play important roles in anthropogenic climate forcing both directly (Bellouin et al., 2005; Carmichael et al., 2009; IPCC, 2013; Scott et al., 2014) and indirectly (Bréon et al., 2002; IPCC, 2013; Penner et al., 2004; Scott et al., 2014) in influencing the global radiation budget. Among the various air pollutants, PM and surface O_3 are the most notorious health threats, as has been stated by several previous studies (Carmichael et al., 2009; Dehghani et al., 2017; Khaniabadi et al., 2017).

With the stated importance of atmospheric aerosols and gases, considerable research efforts have been made to monitor and quantify their amounts in the atmosphere through satellite-, airborne-, and ground-based observations as well as chemistry-transport model (CTM) simulations. In South Korea, the Korean Ministry of the Environment (KMoE) provides real-time chemical concentrations as measured by ground-based observations for six criteria air pollutants (PM_{10}, $PM_{2.5}$, O_3, CO, SO_2, and NO_2) at the Air Korea website (https://www.airkorea.or.kr). In addition, the National Institute of Environmental Research (NIER) of South Korea provides air quality predictions using multiple CTM simulations. Air quality predictions are another crucial element for protecting public health through the forecasting of high air pollution episodes in advance and alerting citizens about these high episodes. In this context, reliable and robust air quality forecasts are necessary to avoid any confusion caused by poor predictions given by CTM simulations.

Although there are various datasets representing air quality, limitations remain in the observations and model outputs. Specifically, observation data are, in general, known to be more accurate than model outputs, but they have spatial and temporal limitations. These limitations will be overcome by improving spatial and temporal coverage via future geostationary satellite instruments such as the Geostationary Environment Monitoring Spectrometer (GEMS) over Asia, the Tropospheric Emissions: Monitoring of Pollution (TEMPO) over North America, and the Sentinel-4 over Europe. In addition, the TROPOspheric Monitoring Instrument (TROPOMI) on board the Copernicus Sentinel-5 Precursor satellite was successfully launched into low earth orbit (LEO) on 13 October 2017 and are providing information on the chemical composition in the atmosphere with a higher spatial resolution of 3.5×7 km^2.

Unlike observation data, models can provide meteorological and chemical information without any spatial and temporal data discontinuity, but they do have an issue of inaccuracy. The major causes of uncertainty in the results of CTM simulations are introduced from imperfect emissions, meteorological fields, initial conditions (ICs), and physical and chemical parameterizations in the models (Carmichael et al., 2008). In order to minimize the limitations and maximize the advantages of observation data and model outputs, there have been numerous attempts to provide accurate and spatially- as well as temporally- continuous information on chemical composition in the atmosphere by integrating observation data with model outputs via data assimilation (DA) techniques.

Although the Korean numerical weather prediction (NWP) carried out by the Korea Meteorological Administration (KMA) employs various DA techniques, almost no previous efforts have been made to develop a air quality prediction system with DA in South Korea.

Therefore, in the present study, the air quality prediction system named as Korean Air Quality Prediction System version 1 (KAQPS v1) was developed by preparing ICs via DA for the Community Multi-scale Air Quality (CMAQ) model (Byun and Schere, 2006; Byun and Ching, 1999) using satellite- and ground-based observations for particulate matter (PM) and atmospheric gases such as CO, O_3, and SO_2. The performances of the system were then demonstrated during the period of the Korea-United States Air Quality Study (KORUS-AQ) campaign (1 May – 12 June 2016) in South Korea.

In this study, the optimal interpolation (OI) method with the Kalman filter was applied in order to develop the air quality prediction system, since this method is still useful and viable in terms of computational cost and performance. The performance of the method is almost comparable to that of the three-dimensional variational (3DVAR) method, as shown in Tang et al. (2017). More complex and advanced DA techniques are currently being and will continue to be applied to current air quality prediction systems. These works are now in progress.

In addition, this manuscript also discusses several practical issues frequently encountered in the air quality predictions such as: i) DA of NO_2 mixing ratios for accurate ozone prediction with a careful consideration of measurement artifacts; ii) the issue of the nocturnal mixing layer height (MLH) for nocturnal predictions; iii) predictions of dust episodes; iv) the use of non-static free parameters; and v) the influences of multiple implementations of the DA before the actual predictions.

The details of the datasets and methodology used in this study are described in Sect. 2. The results of the developed air quality prediction system are discussed in Sect. 3, and then a summary and conclusions are given in Sect. 4.

2. Methodology

The air quality prediction system was developed using the CMAQ model along with meteorological inputs provided by the Weather Research and Forecasting (WRF) model (Skamarock et al., 2008). The ICs for the CMAQ model simulations were prepared via the DA method using satellite-retrieved and ground-based observations. The performances of the developed prediction system were evaluated using ground in-situ data. The models, data, and DA technique are described in detail in the following sections.

2.1 Meteorological and chemistry-transport modeling

2.1.1 WRF model simulations

The WRF model has been developed for providing mesoscale numerical weather prediction (NWP). It has also been used to provide meteorological input fields for CTM simulations (Appel et al., 2010; Chemel et al., 2010; Foley et al., 2010; Lee et al., 2016; Park et al., 2014). In this study, WRF v3.8.1 with the Advanced Research WRF (ARW) dynamical core was applied to prepare the meteorological inputs for the CMAQ model simulations. Dynamical and physical configurations for the WRF model simulations were selected as follows: the Yonsei University (YSU) scheme for planetary boundary layer (Hong et al., 2006); the WRF single-moment 6-class (WSM6) scheme for the micro-physics (Hong and Lim, 2006); the Grell-Freitas ensemble scheme for cumulus parameterization (Grell and Freitas, 2014); the Noah-MP land surface model (Niu et al., 2011; Yang et al., 2011); the rapid radiative transfer model for Global Circulation Models (RRTMG) for shortwave/longwave options (Iacono et al., 2008); and the revised MM5 scheme for surface layer options (Jiménez et al., 2012). The National Centers for Environmental Prediction (NCEP) Final (FNL) Operational Global

159 Analysis data on 1° × 1° grids were chosen for the ICs and boundary conditions (BCs) for the
160 WRF simulations. In order to minimize meteorological field errors for the applications of ICs
161 and BCs to the WRF simulations, the objective analysis (OBSGRID) nudging was conducted
162 using the NCEP Automated Data Processing (ADP) global upper-air/surface observational
163 weather data via the Cressman (1959)'s successive correction method. The adjusted
164 meteorological variables were temperature, geopotential height, relative humidity, and
165 zonal/meridional winds.

166 The model domain for the WRF simulations covers Northeast Asia with a horizontal
167 resolution of 15 × 15 km^2, having a total of 223 latitudinal and 292 longitudinal grid cells. The
168 size of the WRF domain is slightly larger than that of the CMAQ domain, as shown in Fig. 1.
169 The meteorological data have 27 vertical layers from the surface (1000 hPa) to 50 hPa. The
170 WRF meteorological fields (e.g., temperature, pressure, wind, humidity, cloud, etc) were then
171 transformed into the CMAQ-ready format via the Meteorology-Chemistry Interface Processor
172 (MCIP; Otte and Pleim (2010)) v4.3 which is a software to serve for transforming horizontal
173 and vertical coordinates while trying to maintain dynamic consistency between WRF and
174 CMAQ model simulations.

175

176 **2.1.2 CMAQ model simulations**

177 The CMAQ v5.1 model was used to estimate the concentrations of the atmospheric
178 chemical species over the domain, as shown in Fig. 1. The CMAQ domain has 204 latitudinal
179 and 273 longitudinal grid cells in total, and also has a 15 × 15 km^2 horizontal resolution and 27
180 sigma vertical layers. The CMAQv5.1 model was configured to use. Chemical and physical
181 configurations for the CMAQ model simulations were selected as follows: SAPRC07tc for the

gas-phase chemical mechanism (Hutzell et al., 2012); AERO6 for aerosol thermodynamics (Appel et al., 2013); Euler Backward Iterative (EBI) chemistry solver (Hertel et al., 1993), which is a numerically optimized photochemistry mechanism solver; M3DRY for dry deposition velocity (Pleim and Xiu, 2003; Xiu and Pleim, 2001); global mass-conserving scheme (YAMO & WRF) for horizontal and vertical advection (Colella and Woodward, 1984); MULTISCALE (Louis, 1979), which is a simple first-order eddy diffusion scheme for horizontal diffusion; and the Asymmetric Convective Model 2 (ACM2; Pleim, 2007a, 2007b) for vertical diffusion.

For anthropogenic emissions, KORUS v1.0 emissions (Woo et al., 2012) were used. The KORUS v1.0 emissions cover almost all of Asia, and are based on three emission inventories: the Comprehensive Regional Emissions inventory for Atmospheric Transport Experiment (CREATE) for East Asia excluding Japan; the Model Inter-Comparison Study for Asia (MICS-Asia) for Japan; and the Studies of Emissions and Atmospheric Composition, Clouds and Climate Coupling by Regional Surveys (SEAC4RS) for South and Southeast Asia.

Biogenic emissions were prepared by running the Model of Emissions of Gases and Aerosols from Nature (MEGAN v2.1; Guenther et al., 2006; 2012) with a grid size identical to that of the CMAQ model simulations. For the MEGAN simulations, the MODIS land cover data (Friedl et al., 2010) and improved leaf area index (LAI) based on MODIS datasets (Yuan et al., 2011) were utilized. Pyrogenic emissions were obtained from the Fire Inventory from NCAR (FINN; Wiedinmyer et al., 2006, 2011). The lateral BCs for the CMAQ model simulations were prepared using the global model results of the Model for Ozone and Related chemical Tracers version 4 (MOZART-4; Emmons et al., 2010) at every 6 hours. The mapping and re-gridding of the MOZART-4 data were conducted by matching the CMAQ grid

205 information.

206

207 **2.2 Observation data**

208 **2.2.1. Satellite-based observations**

209 A Korean geostationary satellite of Communication, Ocean, and Meteorological
210 Satellite (COMS) was launched on 26 June in 2010 over the Korean Peninsula. The COMS is
211 a geostationary orbit satellite and it is stationed at an altitude of approximately 36,000 km at a
212 latitude of 36°N and a longitude of 128.2°E with a horizontal coverage of 2500 × 2500 km^2
213 (refer to Fig. 1). Among the three payloads of the COMS, Geostationary Ocean Color Image
214 (GOCI) is the first multi-channel ocean color sensor with visible and near infrared channels.
215 The GOCI instrument provides hourly spectral images with a spatial resolution of 500 × 500
216 m^2 from 00:30 to 07:30 Coordinated Universal Time (UTC) for eight spectral (6 visible and 2
217 near-infrared) channels at 412, 443, 490, 555, 660, 680, 745, and 865 nm.

218 The Yonsei aerosol retrieval (YAER) algorithm for the GOCI sensor was initially
219 developed by Lee et al. (2010) to retrieve the aerosol optical properties (AOPs) over ocean
220 areas, and was then improved by expanding to consider non-spherical aerosol optical properties
221 (Lee et al., 2012). Choi et al. (2016) further extended the algorithm for application to land
222 surfaces, and the algorithm was referred to as the GOCI YAER version 1 algorithm. With the
223 GOCI YAER algorithm, hourly Aerosol Optical Depths (AODs) at 550 nm were produced over
224 East Asia. Choi et al. (2016) compared the retrieved GOCI AODs with other satellite-retrieved
225 and ground-based observations, and found several errors in the cloud masking and surface
226 reflectances. These errors were corrected in the recently updated second version of the GOCI
227 YAER algorithm (Choi et al., 2018), which used the updated cloud masking and more accurate
228 surface reflectances. In this study, the most recent GOCI AOD products from the GOCI YAER

version 2 algorithm were used.

2.2.2. Ground-based observations

In addition to the satellite data, ground-based observations in South Korea and China were also collected for use in the air quality prediction system for PM and gas-phase pollutants. The orange, red, and blue dots in Fig. 1 represent the ground-based observation sites in China, Air Korea, and super-site stations in South Korea, respectively. These observations provide real-time concentrations of criteria species such as PM_{10}, $PM_{2.5}$, CO, O_3, SO_2, and NO_2.

Throughout the period of the KORUS-AQ campaign, ground-based observation data were obtained from 1514 stations in China, 264 Air Korea stations, and seven super-site stations in South Korea. In this study, 80 % of the ground-based observations in China and Air Korea stations in South Korea were randomly selected for use in the prediction system. The other 20 % of the data and super-site observations were used to evaluate the performances of the developed air quality prediction system.

In addition, AErosol RObotic NETwork (AERONET) AODs were used to conduct an independent evaluation of the air quality prediction system. AERONET is a federated global ground-based sun photometer network (Holben et al., 1998). Cloud-screened and quality-assured level 2.0 AODs for the AERONET were used in this study.

2.3 Air quality prediction system

In the present study, the air quality prediction system was developed by adjusting the ICs for the CMAQ model simulations based on DA with satellite-retrieved and ground-measured observations. Two parallel WRF-CMAQ model runs were conducted. The first

252 experiment that involved adjusting ICs via DA is referred to as DA RUN (see Fig. 2). In order
253 to evaluate the prediction system, a second experiment, in which the ICs were originated from
254 the previous CMAQ model simulations without assimilations, was also conducted. This
255 CMAQ run is referred to as BASE RUN.
256
257 **2.3.1. AOD calculations**
258 CMAQ AODs are calculated by integrating the aerosol extinction coefficient (σ_{ext})
259 using the following equation:
260
261 $$\mathrm{AOD}(\lambda) = \int_0^z \sigma_{ext}(\lambda)\ \mathrm{dz} \quad (1)$$
262
263 where z represents the vertical height; σ_{ext} is defined as the sum of the absorption coefficient
264 (σ_{abs}) and the scattering coefficient (σ_{sca}); and σ_{abs} and σ_{sca} can be estimated by Eqns (3)
265 and (4), respectively, as shown below:
266
267 $$\sigma_{ext}(\lambda) = \sigma_{abs}(\lambda) + \sigma_{sca}(\lambda) \quad (2)$$
268 $$\sigma_{abs}(\lambda)\ [\mathrm{Mm}^{-1}] = \sum_i^n \sum_j^m \{(1 - \omega_{ij}(\lambda)) \cdot \beta_{ij}(\lambda) \cdot f_{ij}(\mathrm{RH}) \cdot [\mathrm{C}]_{ij}\} \quad (3)$$
269 $$\sigma_{sca}(\lambda)\ [\mathrm{Mm}^{-1}] = \sum_i^n \sum_j^m \{\omega_{ij}(\lambda) \cdot \beta_{ij}(\lambda) \cdot f_{ij}(\mathrm{RH}) \cdot [\mathrm{C}]_{ij}\} \quad (4)$$
270
271 where i and j denote the particulate species and size bin (or particle mode), respectively; $\omega_{ij}(\lambda)$
272 is the single scattering albedo; $\beta_{ij}(\lambda)$ is the mass extinction efficiency (MEE) of particulate
273 species i for the size bin or particle mode j; $[\mathrm{C}]_{ij}$ is the concentration of particulate species
274 including $(NH_4)_2SO_4$, NH_4NO_3, black carbon, organic aerosols (OA), mineral dust, and sea-

275 salt aerosols; RH is the relative humidity; $f_{ij}(RH)$ is the hygroscopic factor; and the single
276 scattering albedo (ω) implies to the fraction (portion) of scattering in the total extinction.
277 Using Eqns. (2) - (4), AODs were calculated from the aerosol composition and RH.
278 These have been intensive tests using different β and f(RH) values in the following three
279 previous studies: (1) Chin et al. (2002)'s study with the Goddard Chemistry Aerosol Radiation
280 and Transport (GOCART) model; (2) Martin et al. (2003)'s study with the GEOS-Chem model;
281 and (3) Malm and Hand (2007)'s study with the CMAQ model. Lee et al. (2016) tested these
282 methods, and then found that Chin et al. (2002)'s method reproduced the best results in
283 estimating AODs at 550 nm over East Asia. On the basis of Lee et al. (2016)'s work, σ_{ext} was
284 estimated with the β and f(RH) values suggested by Chin et al. (2002). After that, σ_{ext} was
285 integrated with respect to altitude, in order to calculate the AODs. The calculated AODs were
286 used in the air quality prediction system in order to prepare the ICs for the PM predictions.
287
288 **2.3.2. Data assimilation (DA)**
289 The ground-based observations, together with GOCI-derived AODs, were used to
290 prepare the ICs for the air quality predictions with the CMAQ model simulations. In order to
291 achieve this, the following steps were taken: (i) the CMAQ-calculated concentrations of CO,
292 O_3, and SO_2 were combined with the concentrations of CO, O_3, and SO_2 obtained from ground-
293 based observations in South Korea (Air Korea) and China; (ii) the CMAQ-calculated AODs
294 were assimilated with the GOCI AODs; (iii) the assimilated AODs were converted into PM_{10};
295 (iv) the converted PM_{10} was again assimilated at the surface in South Korea and China; and (v)
296 after the DA at the surface, the ratios of the assimilated species concentrations to the original
297 CMAQ-simulated concentrations were applied so as to the adjust vertical profiles of the

298 chemical species above the surface. In the air quality prediction system, the DA cycle is 24
299 hours and the assimilation takes place every day at 00:00 UTC (refer to Fig. 3).

300 The optimal interpolation (OI) method with the Kalman filter was chosen in the air
301 quality prediction system. The OI method was originally used for meteorological applications
302 (Lorenc, 1986), and has also been used in the assimilations for trace gases (Khattatov et al.,
303 1999, 2000; Lamarque et al., 1999; Levelt et al., 1998). Recently, the OI technique has also
304 been applied to aerosol fields (Collins et al., 2001; Yu et al., 2003; Generoso et al., 2007;
305 Adhikary et al., 2008; Carmichael et al., 2009; Chung et al., 2010; Park et al., 2011; Park et al.,
306 2014; Tang et al., 2015, 2017).

307 Aerosol assimilation using the OI method was first applied by Collins et al. (2001) as
308 follows:

309

310 $$\tau'_m = \tau_m + \mathbf{K}(\tau_o - \mathbf{H}\tau_m) \quad (5)$$

311 $$\mathbf{K} = \mathbf{B}\mathbf{H}^T(\mathbf{H}\mathbf{B}\mathbf{H}^T + \mathbf{O})^{-1} \quad (6)$$

312 $$\mathbf{O} = [(f_o\tau_o)^2 + (\varepsilon_o)^2]\mathbf{I} \quad (7)$$

313 $$\mathbf{B}(d_x, d_z) = [(f_m\tau_m)^2 + (\varepsilon_m)^2]\exp\left[-\frac{d_x^2}{2l_{mx}^2}\right]\exp\left[-\frac{d_z^2}{2l_{mz}^2}\right] \quad (8)$$

314

315 where τ'_m, τ_m, and τ_o represent the assimilated products by the OI method, the modeled
316 values, and the observed values, respectively; $\mathbf{K}$ is the Kalman gain matrix; $\mathbf{H}$ is the
317 observation operator (or forward operator), which is an interpolator from model to observation
318 space; $\mathbf{B}$ and $\mathbf{O}$ are the background and observation error covariance matrices, respectively;
319 $(\cdot)^T$ denotes the transpose of a matrix; f_o is the fractional error in the observation-retrieved
320 value; ε_o is the minimum root mean square error in the observation-retrieved values; $\mathbf{I}$

denotes the unit matrix; f_m is the fractional error in the model estimates; ε_m is the minimum root mean square error in the model estimates; d_x is the horizontal distance between two model grid points; l_{mx} is the horizontal correlation length scale for the errors in the model; d_z is the vertical distance between two model grid points; and l_{mz} is the vertical correlation length scale for the errors in the model. In this work, the OI technique was applied for the DA of atmospheric gaseous species as well as particulate species.

Six free parameters (f_m, f_o, ε_m, ε_o, l_{mx}, and l_{mz}) were used to calculate the error covariance matrices of the observations and model, the mathematical formalisms of which are described in Eq. (7) and (8), respectively. Several previous studies have used fixed values for free parameters (Collins et al., 2001; Yu et al., 2003; Adhikary et al., 2008; Chung et al., 2010). These runs are called "static" runs. In contrast to those previous studies, "non-static" free parameters were applied in this study by minimizing the differences between the assimilated values and observations via an iterative process at each assimilation time step. This non-static free parameter scheme is possible due to the fact that the OI technique with the Kalman filter is much less costly in terms of computation time than other DA techniques, such as the 3-D or 4-D variational methods. This is another advantage of using the OI technique in this system. It typically takes less than 20 minutes with a workstation environment (dual Intel Xeon 2.40 GHz processor).

2.3.3. Allocation of the assimilated PM_{10} & $PM_{2.5}$ into particulate composition

In the procedure of DA, PM_{10} was assimilated in this study, because the PM_{10} data were more plentiful than $PM_{2.5}$. The assimilated PM_{10} then needs to be allocated into the PM composition for the CMAQ-model prediction runs. In order to achieve this, the differences

between the assimilated PM_{10} and background PM_{10} (ΔPM_{10}) were first calculated. Then, $\Delta PM_{2.5}$ was estimated using the ratios of $PM_{2.5}$ to PM_{10} from the background CMAQ model runs (i.e., $\Delta PM_{2.5}=\Delta PM_{10}\times PM_{2.5}/PM_{10}$). $\Delta PM_{2.5}$ was then allocated to the $PM_{2.5}$ composition according to the comparison between two $PM_{2.5}$ compositions observed at the seven super-sites and simulated from the CMAQ model runs over South Korea. Both of the compositions are shown in Fig. 4. In Fig. 4, "PM OTHERS" indicates the remaining particulate matter species after excluding sulfate, nitrate, ammonium, organic aerosol (OA), and elementary carbon (EC). The PM OTHERS occupies 25 % of the total $PM_{2.5}$ observed at super-sites. The other fraction, $\Delta PM_{10}\times(1-PM_{2.5}/PM_{10})$, was also distributed into the coarse-mode particles ($PM_{2.5-10}$) as crustal elements.

3. Results and discussions

The performances of the air quality prediction system were evaluated by comparing them with ground-based observations from the Air Korea network and super-site stations in South Korea. Several sensitivity analyses were also conducted in order to assess the influences of the DA time-intervals on the accuracy of the air quality prediction.

3.1. Evaluation of the air quality prediction system

3.1.1. Time-series analysis

Figure 5 shows the time-series plots of PM_{10}, $PM_{2.5}$, CO, O_3, and SO_2 concentrations from the BASE RUN and the DA RUN. Here, the observation data (OBS) obtained from the Air Korea network were compared with the results of the two sets of the CMAQ model simulations, i.e., (1) BASE RUN and (2) DA RUN. As mentioned previously, 20% of the Air

Korea observations used in the evaluation were randomly selected during the period of the KORUS-AQ campaign. The other 80 % of the Air Korea data were used in the DA at 00:00 UTC. For the forecast hours from 01:00 to 23:00 UTC, all of the ground observations (254 Air Korea and seven super-site stations) were used to evaluate the performances of the developed air quality prediction system. As shown in Fig. 5, we achieved some improvements in the prediction performances by applying the ICs to the CMAQ model simulations. The BASE RUN significantly under-predicted PM_{10}, $PM_{2.5}$, and CO while the DA RUN produced concentrations that were more consistent with the observations than those of the BASE RUN.

In case of CO, the observed CO mixing ratios were about three times higher than those from the BASE RUN. These large differences are well known, and have been attributed to the underestimated emissions of CO (Heald et al., 2004). However, when the DA was applied, the predictions of the CO mixing ratios improved. Similarly, the performances of the PM_{10} and $PM_{2.5}$ predictions improved with the application of the DA. Unlike PM_{10}, $PM_{2.5}$, and CO, the O_3 mixing ratios and its diurnal trends from both the BASE RUN and DA RUN tend to be well-matched with the observations. By contrast, the poorest performances of the BASE RUN and the DA RUN were shown for SO_2.

In addition, a dust event took place between 6 May and 8 May. This event is captured by the DA RUN (check red peaks in Fig. 5(a) and (b)), while the BASE RUN cannot capture this dust event. This demonstrates the capability of the current system to possibly predict dust events in South Korea. In the DA RUN, dust information is provided into the CMAQ model runs through both/either GOCI AOD and/or ground PM observations measured along the dust plume tracks.

389 The effectiveness of the DA with prediction time was also analyzed by calculating the
390 aggregated average concentrations of atmospheric species (see Figs. 6, 7, and 9). Fig. 6 depicts
391 the CMAQ-calculated average concentrations of PM_{10}, $PM_{2.5}$, CO, and SO_2 against the Air
392 Korea observations. Our air quality prediction system re-generated relatively well-matched
393 concentrations for PM_{10}, $PM_{2.5}$, and CO from the DA RUN.

394 Figure 7 shows the case of ozone from the DA RUN by assimilating CMAQ outputs
395 with Air Korea-observed (a) O_3 mixing ratios, and (b) both O_3 and NO_2 mixing ratios for a
396 preliminary test run. The ozone mixing ratios from the DA RUN in Fig. 7(a) were reasonably
397 consistent with the observations at 00:00 UTC, but disagreed with those between 04:00 and
398 09:00 UTC (13:00 and 18:00 KST), when solar insolation is the most intense. This may be
399 attributed to the chemical imbalances between ozone production and ozone destruction (or
400 titration). However, if CMAQ NO_2 was assimilated with ground-based observations in South
401 Korea (Air Korea) and China, the predicted ozone mixing ratios became substantially closer to
402 the observations, as shown in Fig. 7(b). This is clearly due to the fact that NO_x is an important
403 precursor of ozone. In the prediction of the ozone mixing ratios, both 1-hr peak ozone (around
404 15:00 KST) and 8-hr averaged ozone mixing ratios (between 9:00 and 17:00 KST) are
405 important. Fig. 7 clearly shows that the prediction accuracies of both the ozone mixing ratios
406 were improved after the DA of NO_2 mixing ratios.

407 Although the DA for NO_2 provided better ozone predictions, one should take caution
408 in using the NO_2 observations. The NO_2 mixing ratios measured at Air Korea sites are known
409 to be contaminated by other nitrogen gases such as nitric acid (HNO_3), peroxyacetyl nitrates
410 (PANs), and alkyl nitrates (ANs), since the Air Korea NO_2 mixing ratios are measured through
411 a chemiluminescent method with catalysts of gold or molybdenum oxide at high temperatures.

These are known to be "NO_2 measurement artifacts" (Jung et al., 2017), which is one of the reasons that the DA of NO_2 was not shown in Fig. 6. The NO_2 mixing ratios are corrected from the Air Korea NO_2 data, and are then used to prepare the ICs via the DA for more accurate ozone and NO_2 predictions. Currently, such corrections of the observed NO_2 mixing ratios are being standardized with more sophisticated year-long NO_2 measurements. After the corrections of the NO_2 measurement artifacts, more evolved schemes of ozone and NO_2 predictions will be possible in the future. As shown in Fig. 7, about a 20% reduction (average fraction of non-NO_2 mixing ratios in the observed NO_2 mixing ratios) was made for these demonstration runs (Jung et al., 2017).

Another practical issue is now discussed. Although the assimilation with the observed NO_2 mixing ratios can enhance the accuracy of the predictions of the daytime ozone mixing ratios, the nighttime ozone mixing ratios tend to be consistently over-predicted in the aggregated plot of the ozone mixing ratios at the observation sites (see Fig. 7). This can be caused by underestimated NO_2 mixing ratios and thus not enough nighttime ozone titration. As aforementioned, reliable NO_2 prediction via the correction of the NO_2 measurement artifacts will be made in the future. Another possible reason of the over-predicted ozone mixing ratios during the nighttime can be underestimation of the mixing layer height (MLH). Figure 8 shows a comparison between lidar-measured MLH (black dashed line) and WRF-calculated MLH (with the option of the Yonsei University (YSU) planetary boundary layer scheme by Hong et al. (2006); see red line). As shown in Fig. 8, the nocturnal lidar-measured MLH is about two times higher than the nocturnal WRF-calculated MLH as measured at a lidar site inside the campus of Seoul National University (SNU) in Seoul. Such underestimated MLH in the model tends to compress the ozone molecules within the mixing layer during the nighttime, which

435 leads to consistently over-predicted nocturnal ozone mixing ratios. Based on this discrepancy
436 shown in Fig. 8, more intensive comparison study is being carried out by comparing lidar-
437 measured MLH with model-calculated MLH at multiple sites in South Korea.

438 In this work, the aerosol composition (such as EC, OA, sulfate, nitrate, and ammonium)
439 was further compared with the composition observed at the super-sites shown in Fig. 9. As
440 shown in Fig. 9, agreement was observed between the DA RUN and observations for all of the
441 major PM constituents. Again, a strong capability of our DA system is to improve the
442 predictions of the aerosol composition.

443

444 **3.1.2. Spatial distribution**

445 Figure 10 shows the spatial distributions and bias of PM and chemical species
446 throughout the entire period of the KORUS-AQ campaign over the Seoul Metropolitan Area
447 (SMA). Noticeable improvements are observed to have been achieved in the spatial
448 distributions by applying the ICs into the CMAQ model simulations, particularly for PM_{10} (Fig.
449 10a), $PM_{2.5}$ (Fig. 10b), and CO (Fig. 10c). As shown in Fig. 10, the under-predicted
450 concentrations of PM_{10}, $PM_{2.5}$, and CO were adjusted to concentrations closer to the
451 observations. In case of SO_2 (see Fig. 10d), the DA RUN produced better agreement with the
452 observations than the BASE RUN, but there were still under-predicted SO_2 concentrations over
453 the northeastern part of the SMA.

454 By contrast, relatively lower ozone mixing ratios from the DA RUN against the BASE
455 RUN were found in the southwestern part of the SMA (see Fig. 10e). Due to the nonlinear
456 relationship between NO_x and O_3, high mixing ratios (or emissions) of NO_x in the SMA can
457 lead to depletion of ozone. In these runs, the precursors of ozone such as NO_x and VOCs were

458 excluded in the preparation of the ICs for CMAQ model simulations. Again, this is because the
459 Air Korea NO_2 mixing ratios are contaminated by several reactive nitrogen species, so the data
460 cannot be directly used in the assimilation procedures. In case of VOCs, a limited number of
461 datasets is available in South Korea for the DA. Improvements in the prediction of ozone
462 mixing ratios can be achieved when the NO_2 mixing ratios are corrected and a sufficient
463 number of VOCs data (possibly from satellite data in the future) is available.
464
465 **3.1.3. Statistical analysis**
466 In order to achieve better understanding of the performances of the DA RUN, analyses
467 of statistical variables such as index of agreement (IOA), Pearson's correlation coefficient (R),
468 root mean square error (RMSE), and mean bias (MB) were conducted using observations from
469 the Air Korea stations for PM_{10}, $PM_{2.5}$, CO, SO_2, and O_3 (see Fig. 11). Definitions of the
470 statistical variables are given in Appendix A.
471 After the applications of the ICs, both RMSE and MB became lower, while the
472 correlation coefficient became higher for the entire predictions. In addition, it was found that
473 the differences between the BASE RUN and the DA RUN tended to diminish as the prediction
474 time progressed. The results of the statistical analysis are listed in Table 1. The results of the
475 DA RUN were reasonably consistent with the observations for PM_{10} (IOA = 0.60; R= 0.40;
476 RMSE = 34.87; MB = -13.54) and $PM_{2.5}$ (IOA = 0.71; R= 0.53; RMSE = 17. 83; MB = -2.43),
477 as compared to the BASE RUN for PM_{10} (IOA = 0.51; R= 0.34; RMSE = 40.84; MB = -27.18)
478 and $PM_{2.5}$ (IOA = 0.67; R= 0.51; RMSE = 19.24; MB = -9.9). In terms of bias, an improvement
479 was found for CO: MB = -0.036 for the DA RUN and MB = -0.27 for the BASE RUN.
480 Regarding O_3 and SO_2, the DA RUN showed slightly better performances than the BASE RUN.

Table 2 presents the results of the statistical analysis at 00:00 UTC when the DA was conducted, with the results clearly showing how much closer the DA makes the CMAQ-calculated chemical concentrations to the observed concentrations. Collectively, the DA improved model accuracy by a large degree in terms of R, particularly for PM_{10} (R: 0.3→0.75; slope: 0.17→0.66) and O_3 (R: 0.09→0.61; slope: 0.07→0.42). In addition, for all species, MB and RMSE decreased significantly with the DA RUN as compared with the BASE RUN.

3.2. Sensitivity test of DA time-interval

3.2.1. AOD

In this section, a sensitivity analysis was conducted with different implementation time-intervals of the DA (i.e., 24, 6, and 3 hours) for AOD (refer to Fig. 12). As shown in Fig. 12, more frequent implementation of the DA is expected to make the predicted results closer to the observations. Although the DA RUN with a shorter assimilation time-interval tends to produce a better prediction, it is not always the most appropriate choice, since the shorter assimilation time-interval results in increased computational cost. Therefore, an optimized assimilation time-interval should be found to achieve the best performances from the given DA system with the consideration of its own computational ability.

3.2.2. PM and gases

In addition, sensitivity analyses of the developed air quality prediction system to multiple implementations of the DA with different time-intervals were also investigated for (a) PM_{10}, (b) $PM_{2.5}$, (c) CO, (d) SO_2, and (e) O_3, shown in Fig. 13. Fig. 13 shows a soccer plot analysis for BASE RUN (blue crosses) and DA RUNs with different DA time-intervals of 24

hours (OI; red circles), two hours (2-hr OI; black diamonds), and one hour (1-hr OI; dark-green triangles). This set of testing was designed based on the fact that the performances are expected to improve if the DAs are implemented multiple times prior to the actual predictions at 00:00 UTC. Here, for the 2-hr OI run, the DA was implemented three times a day at 20:00, 22:00, and 00:00 UTC, while for the 1-hr OI run, the DA was implemented at 22:00, 23:00, and 00:00 UTC. The performances of all of the chemical species excluding ozone improved, as expected, with DA RUNs with more frequent and longer DA time-intervals (i.e., three-times implementation with a 2-hr time-interval in our cases). In case of ozone, the best performance was found for the air quality prediction system with the DA time-interval of 24-hr.

Unsurprisingly, more frequent DAs prior to the actual prediction mode (i.e., before 00:00 UTC in our system) with a longer time-interval (such as 2-hr) will be computationally costly. There will certainly be a "trade-off" between the precision of air quality prediction and the computational cost. The system should be designed under the consideration of these two factors.

4. Summary and conclusions

In this study, the air quality prediction system was developed by preparing the ICs for CMAQ model simulations using GOCI AODs and ground-based observations of PM_{10}, CO, ozone, and SO_2 during the period of the KORUS-AQ campaign (1 May – 12 June 2016) in South Korea. The major advantages of the developed air quality prediction system are its comprehensiveness in predicting the ambient concentrations of both gaseous and particulate species (including PM composition) as well as its powerfulness in terms of computational cost.

The performances of the developed prediction system were evaluated using near-surface in-situ observation data. The CMAQ model runs with the ICs (DA RUN) showed higher consistency with the observations of almost all of the chemical species, including PM composition (sulfate, nitrate, ammonium, OA, and EC) and atmospheric gases (CO, ozone, and SO_2), than the CMAQ model runs without the ICs (BASE RUN). Particularly for CO, the DA was able to remarkably improve the model performances, while the BASE RUN significantly under-predicted the CO concentrations (predicting about one-third of the observed values). In case of ozone, both the BASE RUN and DA RUN were in close agreement with observations. More reliable predictions of ozone mixing ratios will be achieved via the DA of the observed NO_2 mixing ratios and the corrections of model-simulated mixing layer height (MLH). For SO_2, the performances of both the BASE RUN and the DA RUN were somewhat poor. Regarding this issue, more accurate SO_2 emissions are required to achieve better SO_2 predictions, and these can be estimated through inverse modeling using satellite data (e.g., Lee et al., 2011). The adjustments of both ICs and emissions may be able to improve the performances of the air quality prediction system, and this will be examined in future studies.

Moreover, the developed air quality prediction system will be upgraded by using the new observation data that will be retrieved after 2020 from the Geostationary Environment Monitoring Spectrometer (GEMS) with a high spatial resolution of 7×8 km^2 as well as a high temporal resolution of 1-hour over a large part of Asia. In addition, the current DA technique of the OI with the Kalman filter can also be upgraded with the use of more advanced DA methods such as variational techniques of 3DVAR and 4DVAR methods, as well as with the ensemble Kalman filter (EnK) method. These research endeavors are currently underway.

548 In conjunction with improving the air quality modeling system, artificial intelligence
549 (AI)-based air quality prediction systems are also currently being developed in several ways
550 (e.g., Kim et al., 2019). Actually, Kim et al. (2019) developed an AI-based PM prediction
551 system based on a deep recurrent neural network (RNN) in South Korea. The AI-based
552 prediction system was optimized by iterative model trainings with the inputs of ground-
553 observed PM_{10}, $PM_{2.5}$, and meteorological fields including wind speed, wind direction, relative
554 humidity, and precipitation. The AI-based prediction system showed better performances at the
555 several sites than the CMAQ model simulations. However, it works only for the observation
556 sites in South Korea where ground-based observations are available. By taking advantages of
557 both the CTM-based air quality prediction and the AI-based prediction systems, both systems
558 will be eventually combined so as to create a more accurate hybrid air quality prediction system
559 over South Korea. This will be the ultimate goal of the series of our research works.

560

561 **Code and data availability.** WRF v3.8.1 (doi:10.5065/D6MK6B4K) and CMAQ v5.1
562 (doi:10.5281/zenodo.1079909) models are both open-source and publicly available. Source
563 codes for WRF and CMAQ can be downloaded at http://www2.mmm.ucar.edu/wrf/users/
564 downloads.html and https://github.com/USEPA/CMAQ, respectively. Data from the KORUS-
565 AQ field campaign can be downloaded from the KORUS-AQ data archive (http://www-
566 air.larc.nasa.gov/missions/korus-aq). Other data were acquired as follows. Ground-based
567 observation data were downloaded from the Air Korea website (http://www.airkorea.or.kr) for
568 South Korea and https://pm25.in for China. AERONET data were downloaded from
569 https://aeronet.gsfc.nasa.gov. The KAQPS v1 code can be obtained by contacting K. Lee

(lkh1515@gmail.com) or from https://github.com/AIR-Codes/KAQPSv1. NCL (2019; doi:10.5065/D6WD3XH5) was used to draw the figures.

Author contributions. KL developed the model code, performed the simulations, and analyzed the results. CHS directed the experiments. JY contributed to shape the research and analysis. SL, MP, HH, and SYP helped analyze the results. MC, JK, YK, JHW, and SWK provided and analyzed data applied in the experiments. KL prepared the manuscript with contributions from all co-authors.

Acknowledgments

This research was supported by the National Strategic Project-Fine particle of the National Research Foundation of Korea (NRF) of the Ministry of Science and ICT (MSIT), the Ministry of Environment (MOE), and the Ministry of Health and Welfare (MOHW) (NRF-2017M3D8A1092022). This work was also funded by the GEMS program of the MOE of the Republic of Korea as part of the Eco Innovation Program of KEITI (2012000160004) and was supported by a grant from the National Institute of Environment Research (NIER), funded by the MOE of the Republic of Korea (NIER-2019-01-01-028). Specially thanks to the entire KORUS-AQ science team for their considerable efforts in conducting the campaign.

APPENDIX A: FORMULAS FOR STATISTICAL EVALUATION INDICES

The formulas used to evaluate the performances of the air quality prediction system are defined as follows.

$$\text{Index Of Agreement (IOA)} = 1 - \frac{\sum_1^n (M - O)^2}{\sum_1^n (|M - \bar{O}| + |O - \bar{O}|)^2} \quad \text{(A1)}$$

$$\text{Correlation Coefficient (R)} = \frac{1}{(n-1)} \sum_1^n \left(\left(\frac{O - \bar{O}}{\sigma_O} \right) \left(\frac{M - \bar{M}}{\sigma_m} \right) \right) \quad \text{(A2)}$$

$$\text{Root Mean Square Error (RMSE)} = \sqrt{\frac{\sum_1^n (M - O)^2}{n}} \quad \text{(A3)}$$

$$\text{Mean Bias (MB)} = \frac{1}{n} \sum_1^n (M - O) \quad \text{(A4)}$$

$$\text{Mean Normalized Bias (MNB)} = \frac{1}{n} \sum_1^n \left(\frac{M - O}{O} \right) \times 100\ \% \quad \text{(A5)}$$

$$\text{Mean Normalized Error (MNE)} = \frac{1}{n} \sum_1^n \left(\frac{|M - O|}{O} \right) \times 100\ \% \quad \text{(A6)}$$

$$\text{Mean Fractional Bias (MFB)} = \frac{1}{n} \sum_1^n \frac{(M - O)}{\left(\frac{M + O}{2} \right)} \times 100\ \% \quad \text{(A7)}$$

606 $$\text{Mean Fractional Error (MFE)} = \frac{1}{n}\sum_{1}^{n}\frac{|M-O|}{\left(\frac{M+O}{2}\right)} \times 100\ \% \quad \text{(B8)}$$

607

608 In Eqns. (A1) - (A8), M and O represent the model and observation data, respectively. N is the
609 number of data points and σ means the standard deviation. The overbars in the equations
610 indicate the arithmetic mean of the data. The units of RMSE and MB are the same as the unit
611 of data, while IOA and R are dimensionless statistical parameters.

612

References

Adhikary, B., Kulkarni, S., Dallura, A., Tang, Y., Chai, T., Leung, L. R., Qian, Y., Chung, C. E., Ramanathan, V. and Carmichael, G. R.: A regional scale chemical transport modeling of Asian aerosols with data assimilation of AOD observations using optimal interpolation technique, Atmospheric Environment, 42(37), 8600–8615, doi:10.1016/j.atmosenv.2008.08.031, 2008.

Appel, K. W., Roselle, S. J., Gilliam, R. C. and Pleim, J. E.: Sensitivity of the Community Multiscale Air Quality (CMAQ) model v4.7 results for the eastern United States to MM5 and WRF meteorological drivers, Geoscientific Model Development, 3, 169–188, 2010.

Appel, K. W., Pouliot, G. A., Simon, H., Sarwar, G., Pye, H. O. T., Napelenok, S. L., Akhtar, F. and Roselle, S. J.: Evaluation of dust and trace metal estimates from the Community Multiscale Air Quality (CMAQ) model version 5.0, Geoscientific Model Development, 6(4), 883–899, doi:10.5194/gmd-6-883-2013, 2013.

Bellouin, N., Boucher, O., Haywood, J. and Reddy, M. S.: Global estimate of aerosol direct radiative forcing from satellite measurements, Nature, 438(7071), 1138–1141, doi:10.1038/nature04348, 2005.

Bréon, F.-M., Tanré, D. and Generoso, S.: Aerosol Effect on Cloud Droplet Size Monitored from Satellite, Science, 295(5556), 834–838, doi:10.1126/science.1066434, 2002.

Byun, D. and Schere, K. L.: Review of the Governing Equations, Computational Algorithms, and Other Components of the Models-3 Community Multiscale Air Quality (CMAQ) Modeling System, Appl. Mech. Rev, 59(2), 51–77, doi:10.1115/1.2128636, 2006.

Byun, D. W. and Ching, J. K. S.: Science algorithms of the EPA models-3 community multiscale air quality (CMAQ) modeling system, U.S. Environmental Protection Agency, EPA/600/R-99/030 (NTIS PB2000-100561)., 1999.

Carmichael, G. R., Sakurai, T., Streets, D., Hozumi, Y., Ueda, H., Park, S. U., Fung, C., Han, Z., Kajino, M., Engardt, M., Bennet, C., Hayami, H., Sartelet, K., Holloway, T., Wang, Z., Kannari, A., Fu, J., Matsuda, K., Thongboonchoo, N. and Amann, M.: MICS-Asia II: The model intercomparison study for Asia Phase II methodology and overview of findings, Atmospheric Environment, 42(15), 3468–3490, doi:10.1016/j.atmosenv.2007.04.007, 2008.

Carmichael, G. R., Adhikary, B., Kulkarni, S., D'Allura, A., Tang, Y., Streets, D., Zhang, Q., Bond, T. C., Ramanathan, V., Jamroensan, A. and Marrapu, P.: Asian Aerosols: Current and Year 2030 Distributions and Implications to Human Health and Regional Climate Change, Environ. Sci. Technol., 43(15), 5811–5817, doi:10.1021/es8036803, 2009.

Chemel, C., Sokhi, R. S., Yu, Y., Hayman, G. D., Vincent, K. J., Dore, A. J., Tang, Y. S., Prain, H. D. and Fisher, B. E. A.: Evaluation of a CMAQ simulation at high resolution over the UK for the calendar year 2003, Atmospheric Environment, 44(24), 2927–2939, doi:10.1016/j.atmosenv.2010.03.029, 2010.

Chin, M., Ginoux, P., Kinne, S., Torres, O., Holben, B. N., Duncan, B. N., Martin, R. V., Logan, J. A., Higurashi, A. and Nakajima, T.: Tropospheric Aerosol Optical Thickness from the GOCART Model and Comparisons with Satellite and Sun Photometer Measurements, J. Atmos. Sci., 59(3), 461–483, doi:10.1175/1520-0469(2002)059<0461:TAOTFT>2.0.CO;2, 2002.

Choi, M., Kim, J., Lee, J., Kim, M., Park, Y.-J., Jeong, U., Kim, W., Hong, H., Holben, B., Eck, T. F., Song, C. H., Lim, J.-H. and Song, C.-K.: GOCI Yonsei Aerosol Retrieval (YAER) algorithm and validation during the DRAGON-NE Asia 2012 campaign, Atmos. Meas. Tech., 9(3), 1377–1398, doi:10.5194/amt-9-1377-2016, 2016.

Choi, M., Kim, J., Lee, J., Kim, M., Park, Y.-J., Holben, B., Eck, T. F., Li, Z. and Song, C. H.: GOCI Yonsei aerosol retrieval version 2 products: an improved algorithm and error analysis with uncertainty estimation from 5-year validation over East Asia, Atmos. Meas. Tech., 11(1), 385–408, doi:10.5194/amt-11-385-2018, 2018.

Chung, C. E., Ramanathan, V., Carmichael, G., Kulkarni, S., Tang, Y., Adhikary, B., Leung, L. R. and Qian, Y.: Anthropogenic aerosol radiative forcing in Asia derived from regional models with atmospheric and aerosol data assimilation, Atmos. Chem. Phys., 10(13), 6007–6024, doi:10.5194/acp-10-6007-2010, 2010.

Colella, P. and Woodward, P. R.: The Piecewise Parabolic Method (PPM) for gas-dynamical simulations, Journal of Computational Physics, 54(1), 174–201, doi:10.1016/0021-9991(84)90143-8, 1984.

Collins, W. D., Rasch, P. J., Eaton, B. E., Khattatov, B. V., Lamarque, J.-F. and Zender, C. S.: Simulating aerosols using a chemical transport model with assimilation of satellite aerosol retrievals: Methodology for INDOEX, J. Geophys. Res., 106(D7), 7313–7336, doi:10.1029/2000JD900507, 2001.

Cressman, G. P.: An operational objective analysis system, Mon. Wea. Rev., 87(10), 367–374, 1959.

Dehghani, M., Keshtgar, L., Javaheri, M. R., Derakhshan, Z., Conti, O., Gea, Zuccarello, P. and Ferrante, M.: The effects of air pollutants on the mortality rate of lung cancer and leukemia, Molecular Medicine Reports, 15(5), 3390–3397, 2017.

Emmons, L. K., Walters, S., Hess, P. G., Lamarque, J.-F., Pfister, G. G., Fillmore, D., Granier, C., Guenther, A., Kinnison, D., Laepple, T., Orlando, J., Tie, X., Tyndall, G., Wiedinmyer, C., Baughcum, S. L. and Kloster, S.: Description and evaluation of the Model for Ozone and Related chemical Tracers, version 4 (MOZART-4), Geosci. Model Dev., 3(1), 43–67, doi:10.5194/gmd-3-43-2010, 2010.

Foley, K. M., Roselle, S. J., Appel, K. W., Bhave, P. V., Pleim, J. E., Otte, T. L., Mathur, R., Sarwar, G., Young, J. O., Gilliam, R. C., Nolte, C. G., Kelly, J. T., Gilliland, A. B. and Bash, J. O.: Incremental testing of the Community Multiscale Air Quality (CMAQ) modeling system version 4.7, Geosci. Model Dev., 3(1), 205–226, doi:10.5194/gmd-3-

689 205-2010, 2010.

690 Friedl, M. A., Sulla-Menashe, D., Tan, B., Schneider, A., Ramankutty, N., Sibley, A. and Huang,
691 X.: MODIS Collection 5 global land cover: Algorithm refinements and characterization
692 of new datasets, Remote Sensing of Environment, 114(1), 168–182,
693 doi:10.1016/j.rse.2009.08.016, 2010.

694 Generoso, S., Bréon, F.-M., Chevallier, F., Balkanski, Y., Schulz, M. and Bey, I.: Assimilation
695 of POLDER aerosol optical thickness into the LMDz-INCA model: Implications for the
696 Arctic aerosol burden, J. Geophys. Res., 112(D2), D02311, doi:10.1029/2005JD006954,
697 2007.

698 Grell, G. A. and Freitas, S. R.: A scale and aerosol aware stochastic convective parameterization
699 for weather and air quality modeling, Atmospheric Chemistry and Physics, 14(10), 5233–
700 5250, doi:https://doi.org/10.5194/acp-14-5233-2014, 2014.

701 Guenther, A., Karl, T., Harley, P., Wiedinmyer, C., Palmer, P. I. and Geron, C.: Estimates of
702 global terrestrial isoprene emissions using MEGAN (Model of Emissions of Gases and
703 Aerosols from Nature), Atmospheric Chemistry and Physics, 6(11), 3181–3210, 2006.

704 Guenther, A. B., Jiang, X., Heald, C. L., Sakulyanontvittaya, T., Duhl, T., Emmons, L. K. and
705 Wang, X.: The Model of Emissions of Gases and Aerosols from Nature version 2.1
706 (MEGAN2.1): an extended and updated framework for modeling biogenic emissions,
707 Geosci. Model Dev., 5(6), 1471–1492, doi:10.5194/gmd-5-1471-2012, 2012.

708 Heald, C. L., Jacob, D. J., Jones, D. B. A., Palmer, P. I., Logan, J. A., Streets, D. G., Sachse, G.
709 W., Gille, J. C., Hoffman, R. N. and Nehrkorn, T.: Comparative inverse analysis of satellite
710 (MOPITT) and aircraft (TRACE-P) observations to estimate Asian sources of carbon
711 monoxide: COMPARATIVE INVERSE ANALYSIS, Journal of Geophysical Research:
712 Atmospheres, 109(D23), doi:10.1029/2004JD005185, 2004.

713 Hertel, O., Berkowicz, R., Christensen, J. and Hov, Ø.: Test of two numerical schemes for use
714 in atmospheric transport-chemistry models, Atmospheric Environment. Part A. General
715 Topics, 27(16), 2591–2611, doi:10.1016/0960-1686(93)90032-T, 1993.

716 Holben, B. N., Eck, T. F., Slutsker, I., Tanré, D., Buis, J. P., Setzer, A., Vermote, E., Reagan, J.
717 A., Kaufman, Y. J., Nakajima, T., Lavenu, F., Jankowiak, I. and Smirnov, A.:
718 AERONET—A Federated Instrument Network and Data Archive for Aerosol
719 Characterization, Remote Sensing of Environment, 66(1), 1–16, doi:10.1016/S0034-
720 4257(98)00031-5, 1998.

721 Hong, S.-Y. and Lim, J.-O. J.: The WRF single-moment 6-class microphysics scheme (WSM6),
722 J. Korean Meteor. Soc., 42(2), 129–151, 2006.

723 Hong, S.-Y., Noh, Y. and Dudhia, J.: A New Vertical Diffusion Package with an Explicit
724 Treatment of Entrainment Processes, Mon. Wea. Rev., 134(9), 2318–2341,
725 doi:10.1175/MWR3199.1, 2006.

Hutzell, W. T., Luecken, D. J., Appel, K. W. and Carter, W. P. L.: Interpreting predictions from the SAPRC07 mechanism based on regional and continental simulations, Atmospheric Environment, 46, 417–429, doi:10.1016/j.atmosenv.2011.09.030, 2012.

Iacono, M. J., Delamere, J. S., Mlawer, E. J., Shephard, M. W., Clough, S. A. and Collins, W. D.: Radiative forcing by long-lived greenhouse gases: Calculations with the AER radiative transfer models, J. Geophys. Res., 113(D13), D13103, doi:10.1029/2008JD009944, 2008.

IPCC: Climate Change 2013: The Physical Science Basis. The Fifth Assessment Report of the Intergovernmental Panel on Climate Change, , Cambridge University Press, Cambridge, United Kingdom and New York, NY, USA, 2013.

Jiménez, P. A., Dudhia, J., González-Rouco, J. F., Navarro, J., Montávez, J. P. and García-Bustamante, E.: A Revised Scheme for the WRF Surface Layer Formulation, Monthly Weather Review, 140(3), 898–918, 2012.

Jung, J., Lee, J., Kim, B. and Oh, S.: Seasonal variations in the NO2 artifact from chemiluminescence measurements with a molybdenum converter at a suburban site in Korea (downwind of the Asian continental outflow) during 2015–2016, Atmospheric Environment, 165, 290–300, doi:10.1016/j.atmosenv.2017.07.010, 2017.

Khaniabadi, Y. O., Goudarzi, G., Daryanoosh, S. M., Borgini, A., Tittarelli, A. and De Marco, A.: Exposure to PM10, NO2, and O3 and impacts on human health, Environmental Science and Pollution Research, 24(3), 2781–2789, doi:10.1007/s11356-016-8038-6, 2017.

Khattatov, B. V., Gille, J. C., Lyjak, L. V., Brasseur, G. P., Dvortsov, V. L., Roche, A. E. and Waters, J. W.: Assimilation of photochemically active species and a case analysis of UARS data, J. Geophys. Res., 104(D15), 18715–18737, doi:10.1029/1999JD900225, 1999.

Khattatov, B. V., Lamarque, J.-F., Lyjak, L. V., Menard, R., Levelt, P., Tie, X., Brasseur, G. P. and Gille, J. C.: Assimilation of satellite observations of long-lived chemical species in global chemistry transport models, J. Geophys. Res., 105(D23), 29135–29144, doi:10.1029/2000JD900466, 2000.

Kim, H. S., Park, I., Song, C. H., Lee, K., Yun, J. W., Kim, H. K., Jeon, M., Lee, J. and Han, K. M.: Development of a daily PM10 and PM2.5 prediction system using a deep long short-term memory neural network model, Atmos. Chem. Phys., 19(20), 12935–12951, doi:10.5194/acp-19-12935-2019, 2019.

Lamarque, J.-F., Khattatov, B. V., Gille, J. C. and Brasseur, G. P.: Assimilation of Measurement of Air Pollution from Space (MAPS) CO in a global three-dimensional model, J. Geophys. Res., 104(D21), 26209–26218, doi:10.1029/1999JD900807, 1999.

Lee, C., Martin, R. V., Donkelaar, A. van, Lee, H., Dickerson, R. R., Hains, J. C., Krotkov, N., Richter, A., Vinnikov, K. and Schwab, J. J.: SO2 emissions and lifetimes: Estimates from

763 inverse modeling using in situ and global, space-based (SCIAMACHY and OMI)
764 observations, Journal of Geophysical Research: Atmospheres, 116(D6),
765 doi:10.1029/2010JD014758, 2011.

766 Lee, J., Kim, J., Song, C. H., Ryu, J.-H., Ahn, Y.-H. and Song, C. K.: Algorithm for retrieval of
767 aerosol optical properties over the ocean from the Geostationary Ocean Color Imager,
768 Remote Sensing of Environment, 114(5), 1077–1088, doi:10.1016/j.rse.2009.12.021,
769 2010.

770 Lee, J., Kim, J., Yang, P. and Hsu, N. C.: Improvement of aerosol optical depth retrieval from
771 MODIS spectral reflectance over the global ocean using new aerosol models archived
772 from AERONET inversion data and tri-axial ellipsoidal dust database, Atmos. Chem.
773 Phys., 12(15), 7087–7102, doi:10.5194/acp-12-7087-2012, 2012.

774 Lee, S., Song, C. H., Park, R. S., Park, M. E., Han, K. M., Kim, J., Choi, M., Ghim, Y. S. and
775 Woo, J.-H.: GIST-PM-Asia v1: development of a numerical system to improve particulate
776 matter forecasts in South Korea using geostationary satellite-retrieved aerosol optical data
777 over Northeast Asia, Geosci. Model Dev., 9(1), 17–39, doi:10.5194/gmd-9-17-2016, 2016.

778 Levelt, P. F., Khattatov, B. V., Gille, J. C., Brasseur, G. P., Tie, X. X. and Waters, J. W.:
779 Assimilation of MLS ozone measurements in the global three-dimensional chemistry
780 transport model ROSE, Geophys. Res. Lett., 25(24), 4493–4496,
781 doi:10.1029/1998GL900152, 1998.

782 Lorenc, A. C.: Analysis methods for numerical weather prediction, Q.J.R. Meteorol. Soc.,
783 112(474), 1177–1194, doi:10.1002/qj.49711247414, 1986.

784 Louis, J.-F.: A parametric model of vertical eddy fluxes in the atmosphere, Boundary-Layer
785 Meteorol, 17(2), 187–202, doi:10.1007/BF00117978, 1979.

786 Malm, W. C. and Hand, J. L.: An examination of the physical and optical properties of aerosols
787 collected in the IMPROVE program, Atmospheric Environment, 41(16), 3407–3427,
788 doi:10.1016/j.atmosenv.2006.12.012, 2007.

789 Martin, R. V., Jacob, D. J., Yantosca, R. M., Chin, M. and Ginoux, P.: Global and regional
790 decreases in tropospheric oxidants from photochemical effects of aerosols, J. Geophys.
791 Res., 108(D3), 4097, doi:10.1029/2002JD002622, 2003.

792 NCL: The NCAR Command Language (Version 6.6.2) [Software]. Boulder, Colorado:
793 UCAR/NCAR/CISL/TDD. http://dx.doi.org/10.5065/D6WD3XH5, 2019.

794 Niu, G.-Y., Yang, Z.-L., Mitchell, Kenneth. E., Chen, F., Ek, M. B., Barlage, M., Kumar, A.,
795 Manning, K., Niyogi, D., Rosero, E., Tewari, M. and Xia, Y.: The community Noah land
796 surface model with multiparameterization options (Noah-MP): 1. Model description and
797 evaluation with local-scale measurements, J. Geophys. Res., 116(D12109),
798 doi:10.1029/2010JD015140, 2011.

799 Otte, T. L. and Pleim, J. E.: The Meteorology-Chemistry Interface Processor (MCIP) for the

CMAQ modeling system: updates through MCIPv3.4.1, Geoscientific Model Development, 3(1), 243–256, doi:https://doi.org/10.5194/gmd-3-243-2010, 2010.

Park, M. E., Song, C. H., Park, R. S., Lee, J., Kim, J., Lee, S., Woo, J.-H., Carmichael, G. R., Eck, T. F., Holben, B. N., Lee, S.-S., Song, C. K. and Hong, Y. D.: New approach to monitor transboundary particulate pollution over Northeast Asia, Atmos. Chem. Phys., 14(2), 659–674, doi:10.5194/acp-14-659-2014, 2014.

Park, R. S., Song, C. H., Han, K. M., Park, M. E., Lee, S.-S., Kim, S.-B. and Shimizu, A.: A study on the aerosol optical properties over East Asia using a combination of CMAQ-simulated aerosol optical properties and remote-sensing data via a data assimilation technique, Atmos. Chem. Phys., 11(23), 12275–12296, doi:10.5194/acp-11-12275-2011, 2011.

Penner, J. E., Dong, X. and Chen, Y.: Observational evidence of a change in radiative forcing due to the indirect aerosol effect, Nature, 427(6971), 231–234, doi:10.1038/nature02234, 2004.

Pleim, J. E.: A Combined Local and Nonlocal Closure Model for the Atmospheric Boundary Layer. Part I: Model Description and Testing, J. Appl. Meteor. Climatol., 46(9), 1383–1395, doi:10.1175/JAM2539.1, 2007a.

Pleim, J. E.: A Combined Local and Nonlocal Closure Model for the Atmospheric Boundary Layer. Part II: Application and Evaluation in a Mesoscale Meteorological Model, J. Appl. Meteor. Climatol., 46(9), 1396–1409, doi:10.1175/JAM2534.1, 2007b.

Pleim, J. E. and Xiu, A.: Development of a Land Surface Model. Part II: Data Assimilation, J. Appl. Meteor., 42(12), 1811–1822, doi:10.1175/1520-0450(2003)042<1811:DOALSM>2.0.CO;2, 2003.

Scott, C. E., Rap, A., Spracklen, D. V., Forster, P. M., Carslaw, K. S., Mann, G. W., Pringle, K. J., Kivekäs, N., Kulmala, M., Lihavainen, H. and Tunved, P.: The direct and indirect radiative effects of biogenic secondary organic aerosol, Atmos. Chem. Phys., 14(1), 447–470, doi:10.5194/acp-14-447-2014, 2014.

Skamarock, C., Klemp, B., Dudhia, J., Gill, O., Barker, D., Duda, G., Huang, X., Wang, W. and Powers, G.: A Description of the Advanced Research WRF Version 3, , doi:10.5065/D68S4MVH, 2008.

Tang, Y., Chai, T., Pan, L., Lee, P., Tong, D., Kim, H.-C. and Chen, W.: Using optimal interpolation to assimilate surface measurements and satellite AOD for ozone and PM2.5: A case study for July 2011, Journal of the Air & Waste Management Association, 65(10), 1206–1216, doi:10.1080/10962247.2015.1062439, 2015.

Tang, Y., Pagowski, M., Chai, T., Pan, L., Lee, P., Baker, B., Kumar, R., Delle Monache, L., Tong, D. and Kim, H.-C.: A case study of aerosol data assimilation with the Community Multi-scale Air Quality Model over the contiguous United States using 3D-Var and

837 optimal interpolation methods, Geosci. Model Dev., 10(12), 4743–4758,
838 doi:10.5194/gmd-10-4743-2017, 2017.

839 Wiedinmyer, C., Quayle, B., Geron, C., Belote, A., McKenzie, D., Zhang, X., O'Neill, S. and
840 Wynne, K. K.: Estimating emissions from fires in North America for air quality modeling,
841 Atmospheric Environment, 40(19), 3419–3432, doi:10.1016/j.atmosenv.2006.02.010,
842 2006.

843 Wiedinmyer, C., Akagi, S., Yokelson, R., Emmons, L., Al-Saadi, J., Orlando, J. and Soja, A.:
844 The Fire INventory from NCAR (FINN): A High Resolution Global Model to Estimate
845 the Emissions from Open Burning, Geoscientific Model Development, 625–641, 2011.

846 Woo, J.-H., Choi, K.-C., Kim, H. K., Baek, B. H., Jang, M., Eum, J.-H., Song, C. H., Ma, Y.-
847 I., Sunwoo, Y., Chang, L.-S. and Yoo, S. H.: Development of an anthropogenic emissions
848 processing system for Asia using SMOKE, Atmospheric Environment, 58, 5–13,
849 doi:10.1016/j.atmosenv.2011.10.042, 2012.

850 Xiu, A. and Pleim, J. E.: Development of a Land Surface Model. Part I: Application in a
851 Mesoscale Meteorological Model, J. Appl. Meteor., 40(2), 192–209, doi:10.1175/1520-
852 0450(2001)040<0192:DOALSM>2.0.CO;2, 2001.

853 Yang, Z.-L., Niu, G.-Y., Mitchell, Kenneth. E., Chen, F., Ek, M. B., Barlage, M., Longuevergne,
854 L., Manning, K., Niyogi, D., Tewari, M. and Xia, Y.: The community Noah land surface
855 model with multiparameterization options (Noah-MP): 2. Evaluation over global river
856 basins, J. Geophys. Res., 116(D12110), doi:10.1029/2010JD015139, 2011.

857 Yu, H., Dickinson, R. E., Chin, M., Kaufman, Y. J., Holben, B. N., Geogdzhayev, I. V. and
858 Mishchenko, M. I.: Annual cycle of global distributions of aerosol optical depth from
859 integration of MODIS retrievals and GOCART model simulations, J. Geophys. Res.,
860 108(D3), 4128, doi:10.1029/2002JD002717, 2003.

861 Yuan, H., Dai, Y., Xiao, Z., Ji, D. and Shangguan, W.: Reprocessing the MODIS Leaf Area
862 Index products for land surface and climate modelling, Remote Sensing of Environment,
863 115(5), 1171–1187, doi:10.1016/j.rse.2011.01.001, 2011.

864

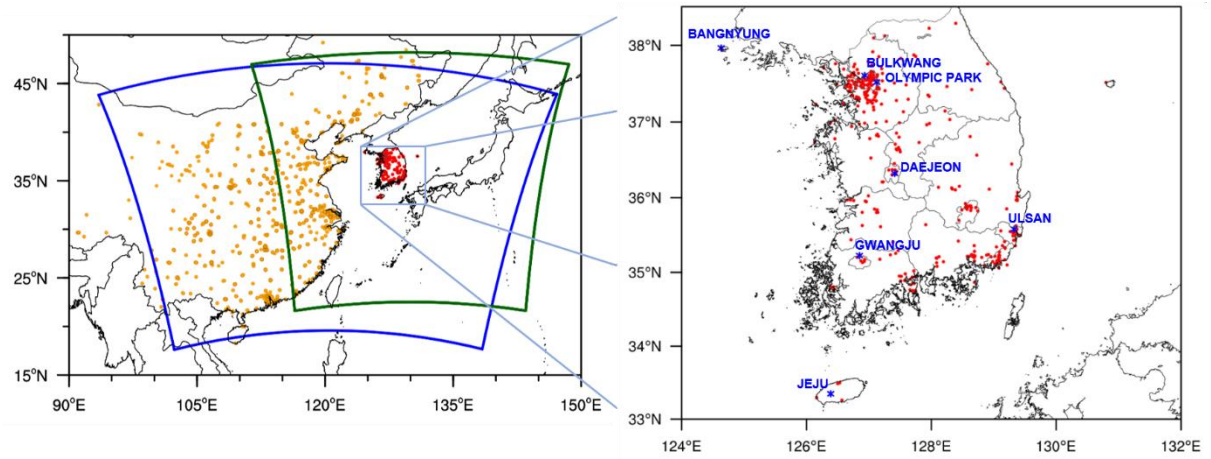

865

866 **Figure 1.** Domains of GOCI sensor (dark green line) and CMAQ model simulations (blue line).
867 Red-colored dots denote the locations of Air Korea sites in South Korea. Orange-colored dots
868 represent the locations of ground-based observation stations in China. Blue stars show the
869 locations of seven super-sites in South Korea. During the KORUS-AQ campaign, observation
870 data were obtained from 1514 stations in China as well as 264 Air Korea and seven super-site
871 stations in South Korea. NCL (2019) was used to draw this figure.

872

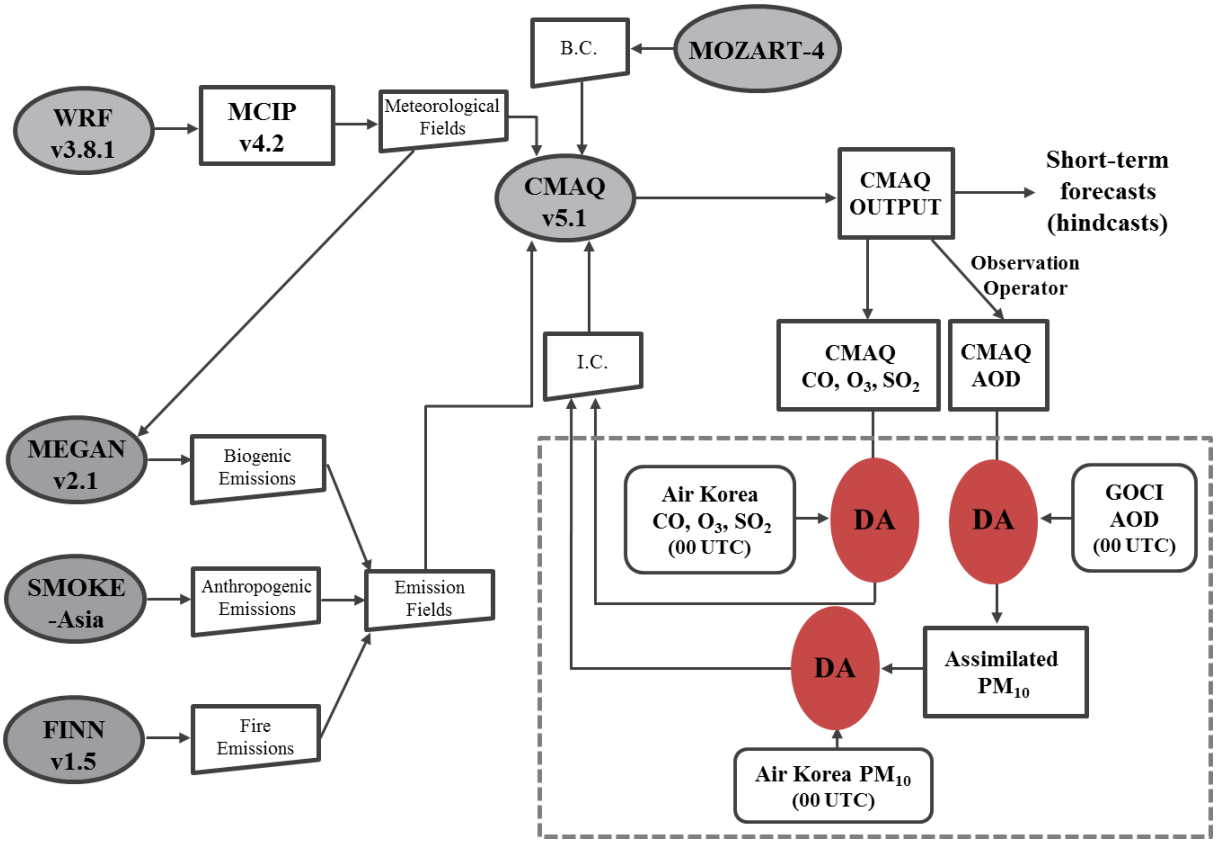

873

874 **Figure 2.** Schematic diagram of the Korean air quality prediction system developed in this
875 study. The initial conditions (ICs) of the CMAQ model simulations are prepared by assimilating
876 CMAQ outputs with satellite-retrieved and ground-measured observations. The data process
877 for preparing the ICs is shown in the box with gray-dashed lines.

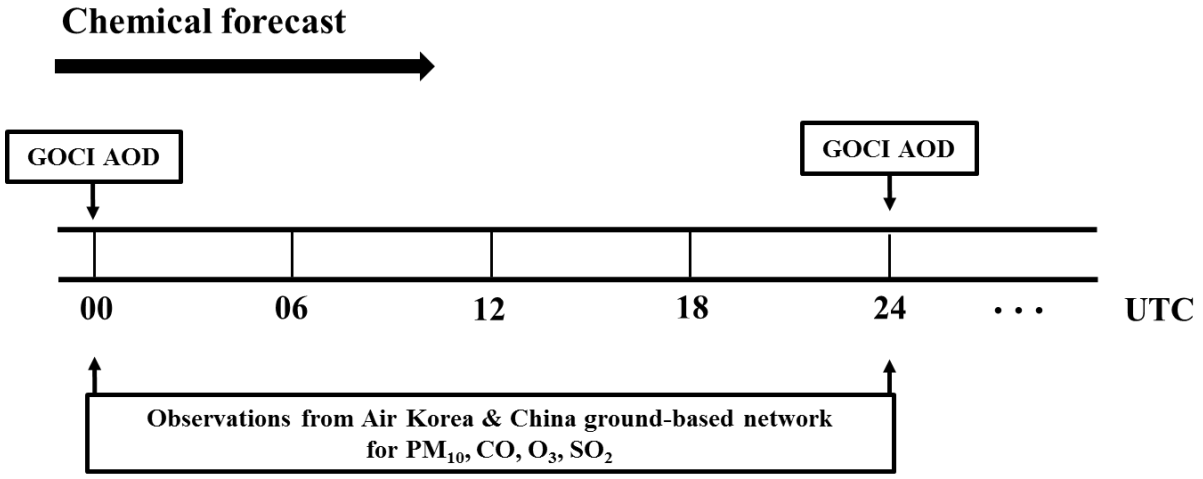

878

879 **Figure 3.** Schematic diagram of the Korean air quality prediction system for particulate matter
880 (PM) and gas-phase pollutants. The data assimilation (DA) cycle is 24 hours for both PM and
881 gas-phase pollutants such as CO, O_3, and SO_2. The DA of NO_2 is excluded in the current study,
882 the reason for which is discussed in the text.

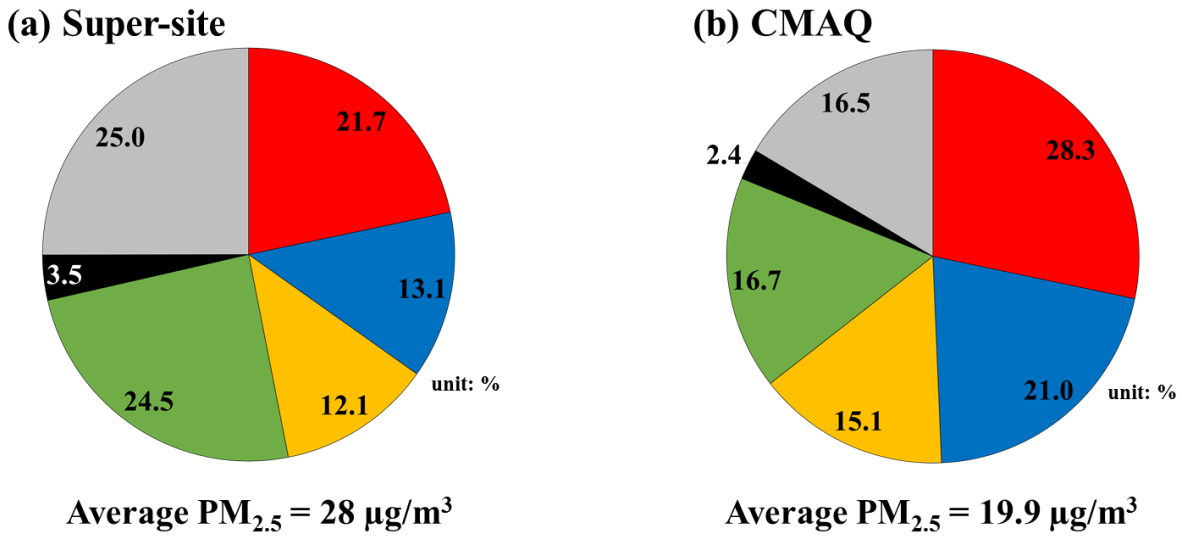

Figure 4. Average $PM_{2.5}$ composition (a) observed at the super-site stations and (b) simulated by the CMAQ model during the KORUS-AQ campaign. The averaged $PM_{2.5}$ measured from the super-sites and calculated from the CMAQ model simulations over the period of the KORUS-AQ campaign are 28 µg/m^3 and 19.9 µg/m^3, respectively. The mass of organic aerosols (OAs) was calculated by multiplying organic carbon mass by 1.6.

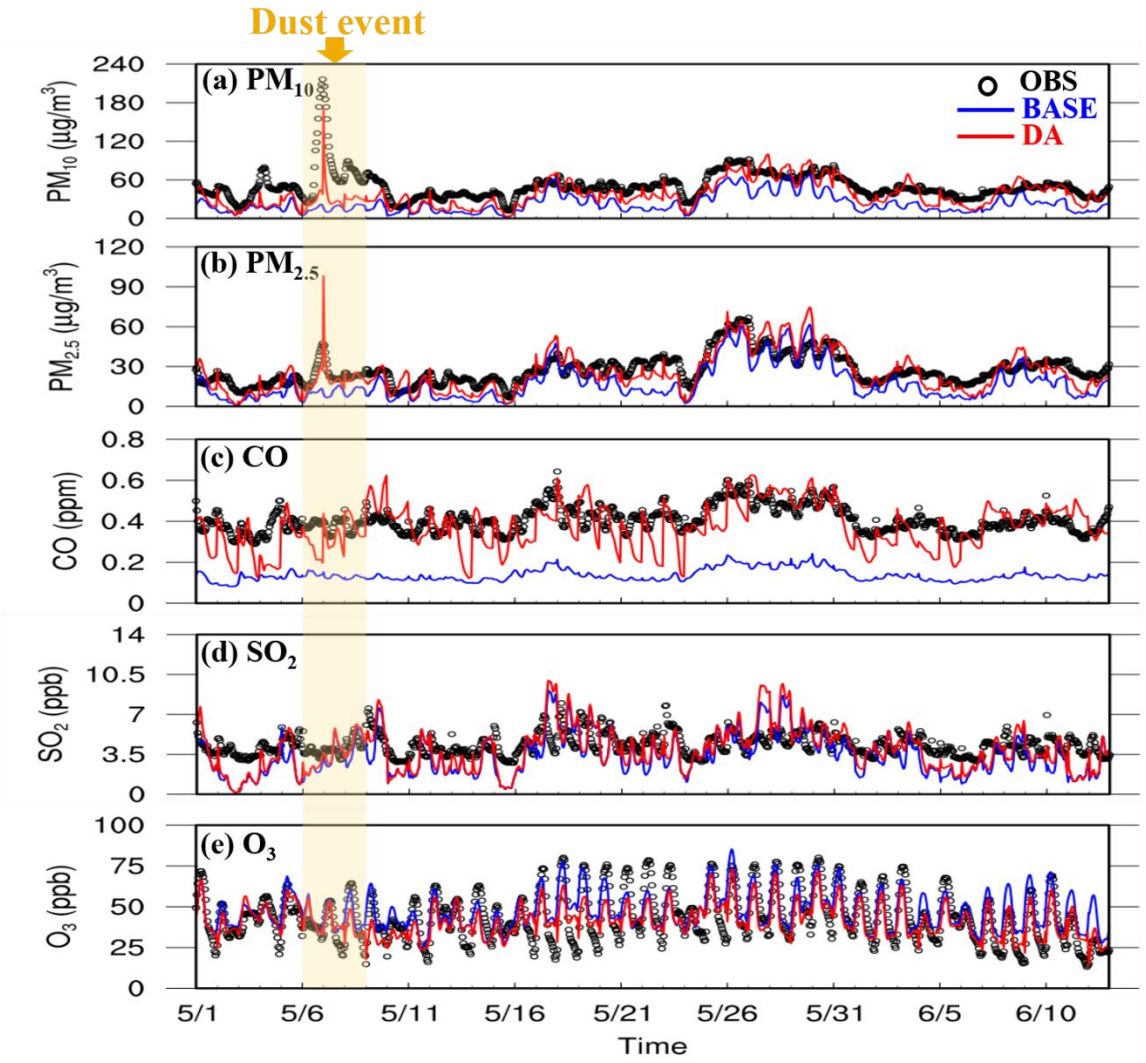

Figure 5. Time-series plots of hourly (a) PM_{10}, (b) $PM_{2.5}$, (c) CO, (d) SO_2, and (e) O_3 concentrations at 264 Air Korea stations. Black open circles (OBS) represent the observed concentrations. Blue and red lines show the results simulated from the BASE RUN and DA RUN over South Korea, respectively.

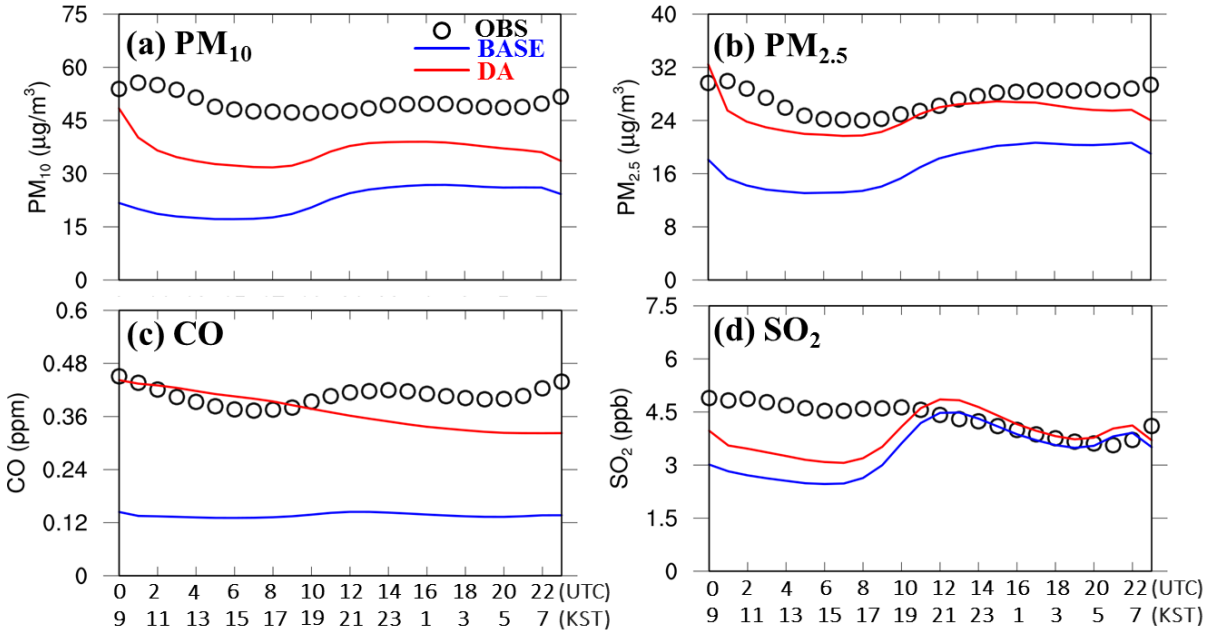

894

895 **Figure 6.** Aggregated average concentrations of (a) PM_{10}, (b) $PM_{2.5}$, (c) CO, and (d) SO_2 at
896 264 Air Korea stations over the KORUS-AQ campaign period. Open black circles denote the
897 observations obtained from 264 Air Korea stations in South Korea. Blue and red lines represent
898 the predicted concentrations from the BASE RUN and DA RUN, respectively. The DA was
899 conducted at 00:00 UTC every day throughout the KORUS-AQ campaign period.

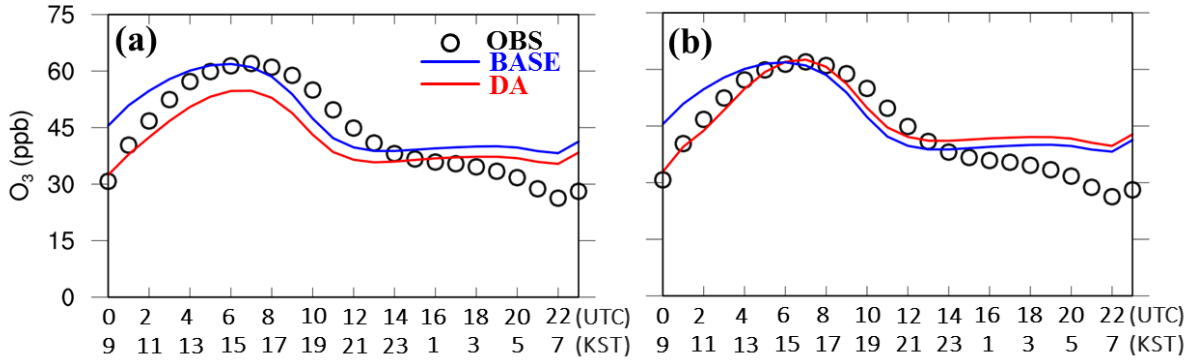

Figure 7. Comparison of CMAQ-simulated O_3 mixing ratios (BASE RUN with blue lines and DA RUN with red lines) with O_3 mixing ratios from Air Korea stations (open black circles). DA RUN was carried out by assimilating CMAQ outputs with Air Korea observations using (a) only O_3 mixing ratios and (b) both O_3 and NO_2 mixing ratios.

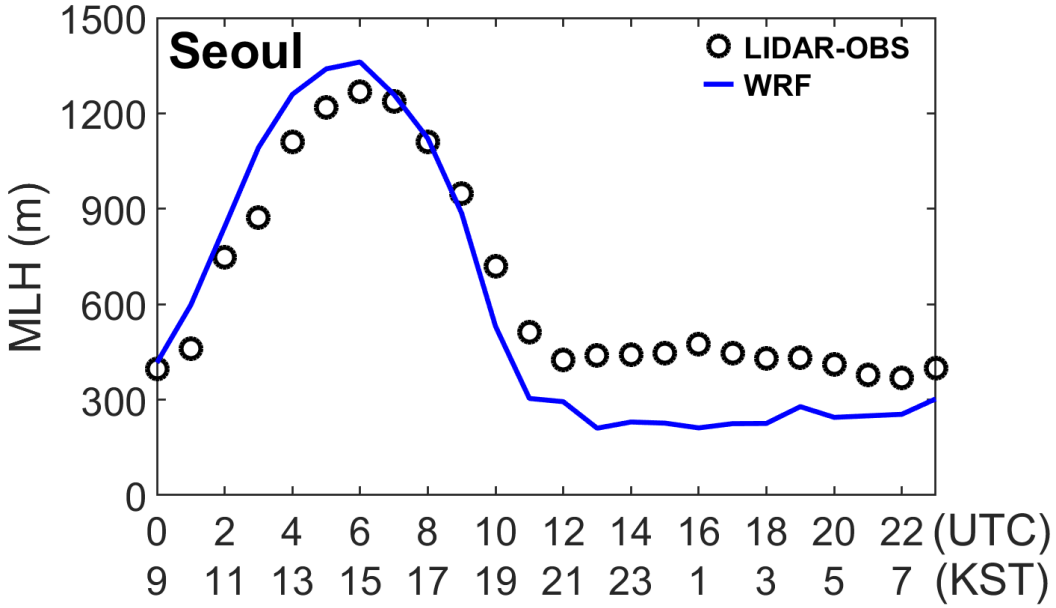

Figure 8. Comparison of WRF-simulated mixing layer height (MLH) (denoted by blue-dashed line) with lidar-measured MLH (denoted by open black circles) at Seoul National University (SNU) in Seoul. KST stands for Korean standard time.

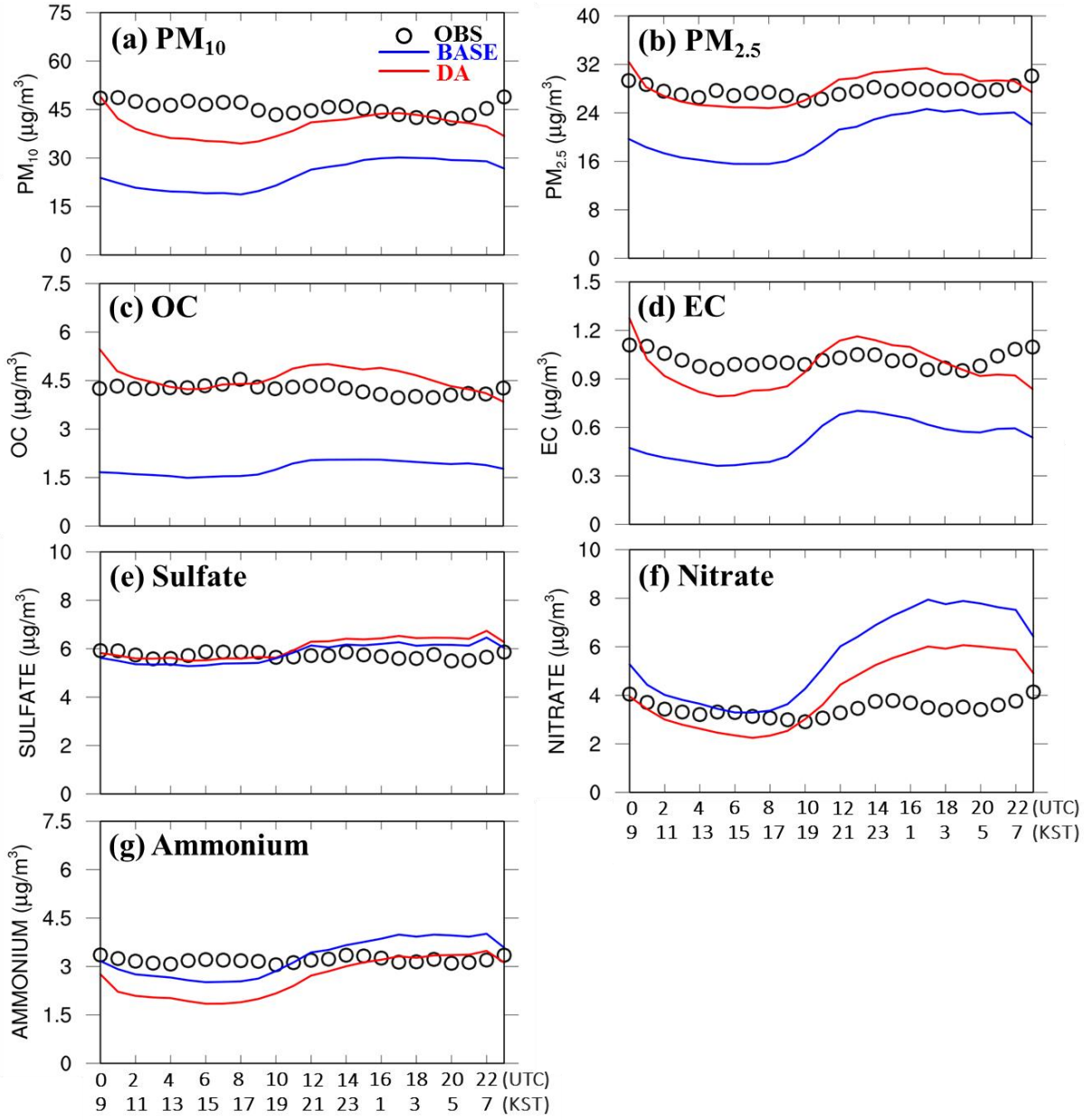

Figure 9. Aggregated average concentrations of (a) PM_{10}, (b) $PM_{2.5}$, (c) OC, (d) EC, (e) sulfate, (f) nitrate, and (g) ammonium as predicted by CMAQ model during the period of the KORUS-AQ campaign. The others are the same as those shown in Fig. 7, except for the fact that the observation data used here were obtained from the seven super-site stations in South Korea.

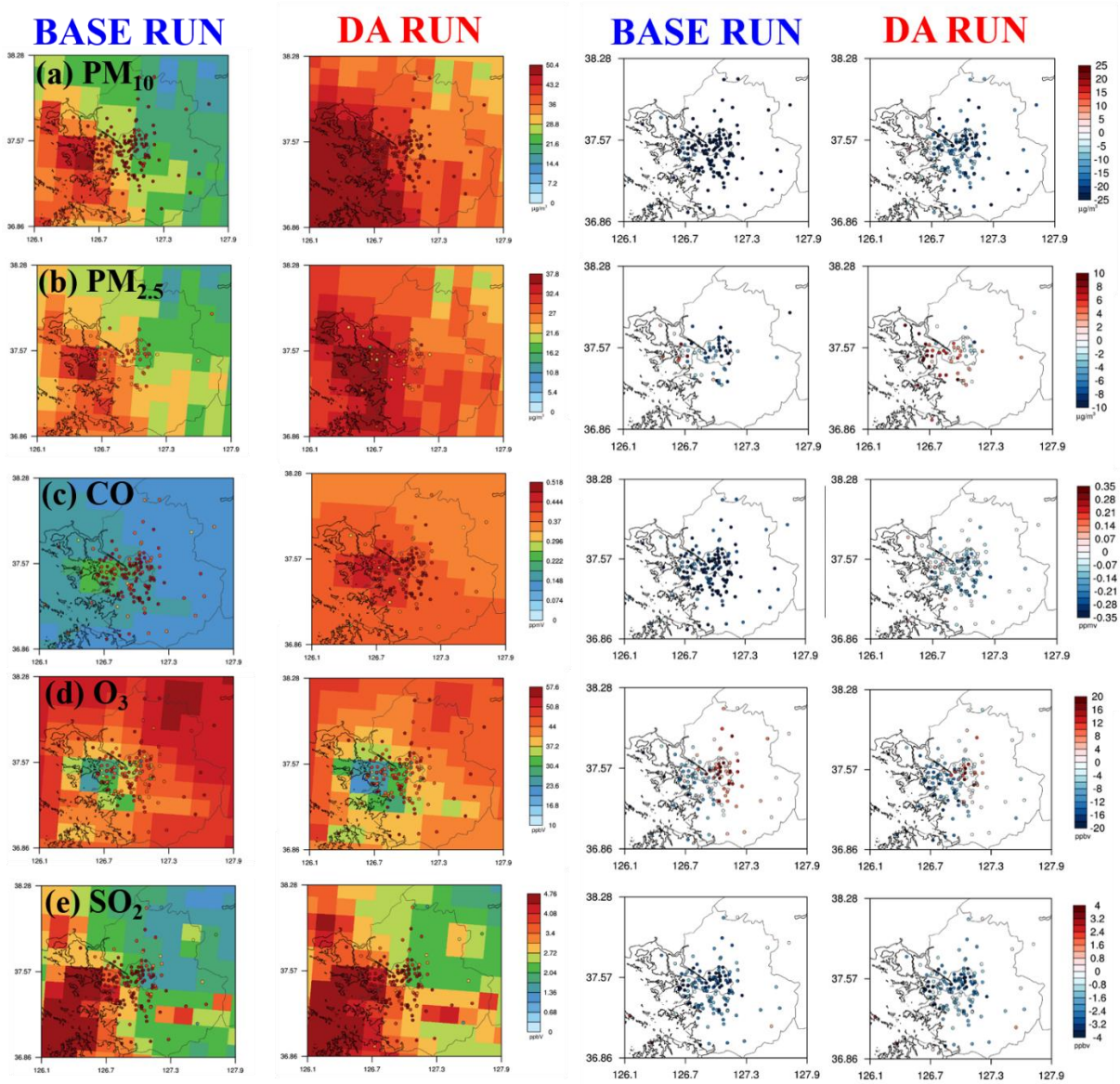

915

916 **Figure 10.** Spatial distributions (first and second columns) and bias (third and fourth columns)
917 of (a) PM_{10}, (b) $PM_{2.5}$, (c) CO, (d) SO_2, and (e) O_3 over Seoul Metropolitan Area (SMA) for
918 the entire period of the KORUS-AQ campaign. Colored circles of first and second columns
919 represent the concentrations of the air pollutants observed at the Air Korea stations in the SMA.

920

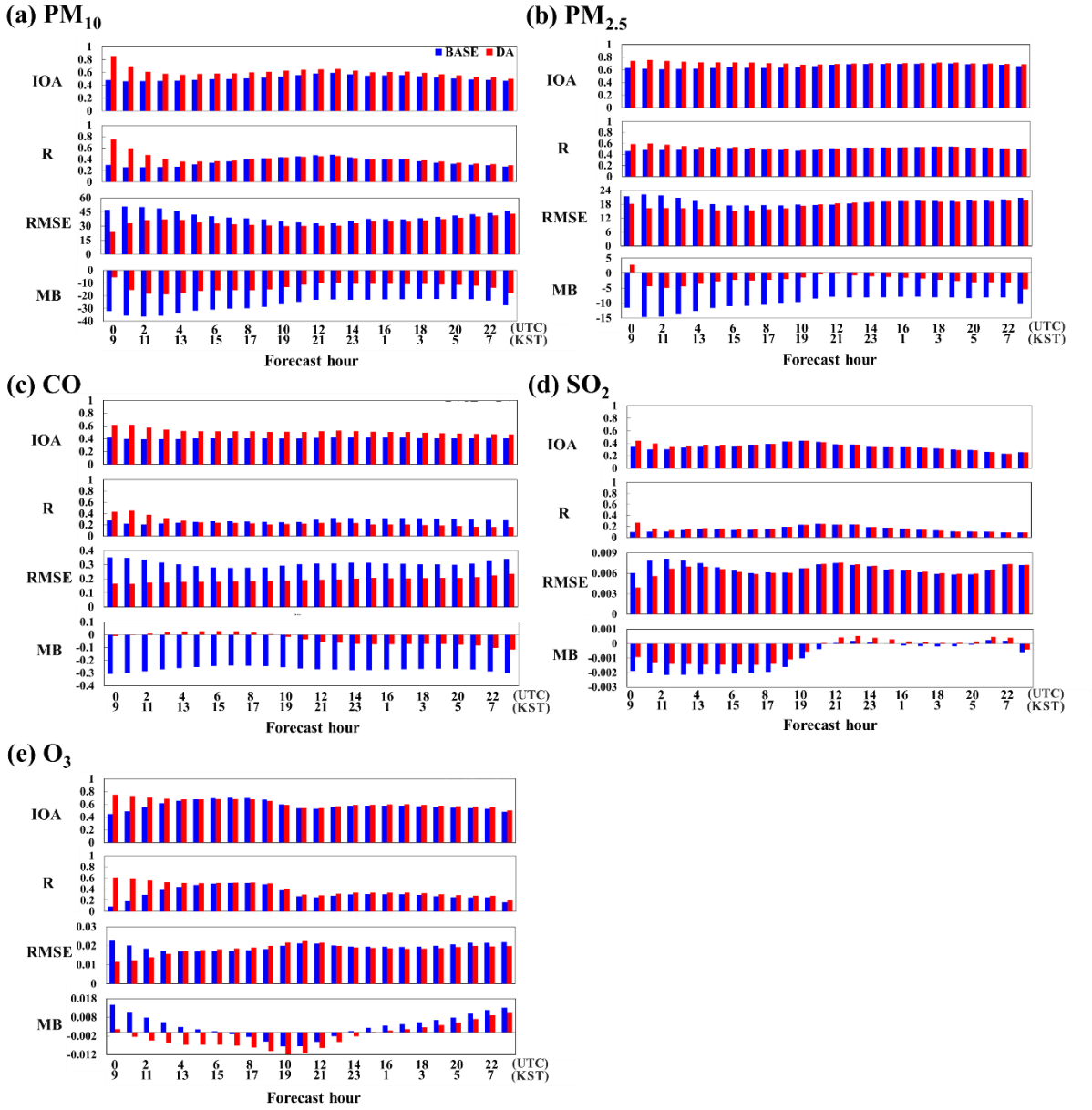

921

922 **Figure 11.** Time-series plots of four performance metrics (IOA, R, RMSE, and MB) for (a)
923 PM_{10}, (b) $PM_{2.5}$, (c) CO, (d) SO_2, and (e) O_3 forecasts. The DA was conducted at 00:00 UTC.
924 The units of RMSE and MB are $\mu g/m^3$ and ppmv for PM concentrations and for gaseous species,
925 respectively. The definitions of the four performance metrics are shown in Appendix A.

926

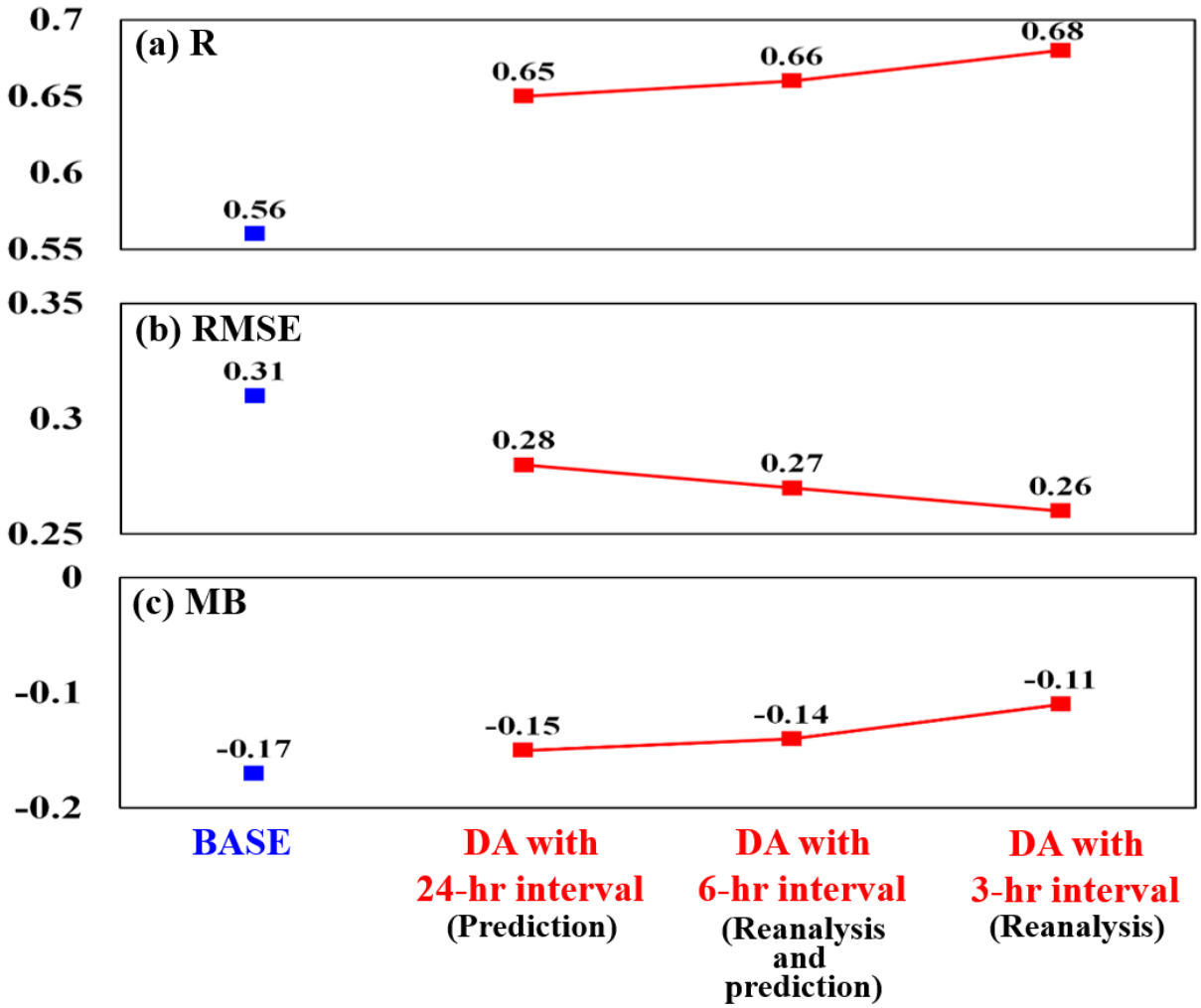

927

928 **Figure 12.** Variations of three performance metrics (R, RMSE, and MB) with time-intervals of
929 data assimilations. For these tests, the GOCI AODs were used in the DA to update the initial
930 conditions of the CMAQ model simulations. The results from the three CMAQ model
931 simulations were compared with AERONET AODs ("ground truth"). The two blue squares
932 represent the performances from the BASE RUNs and the red squares indicate the
933 performances from the DA RUNs. The three experiments were carried out with the assimilation
934 time-intervals of 24, 6, and 3 hours (hr), respectively. Here, the DA RUN with the 24-hr time-
935 interval is referred to as "air quality prediction", and the DA RUNs with the 6-hr and 3-hr time-
936 interval are referred to as "air quality reanalysis".

937

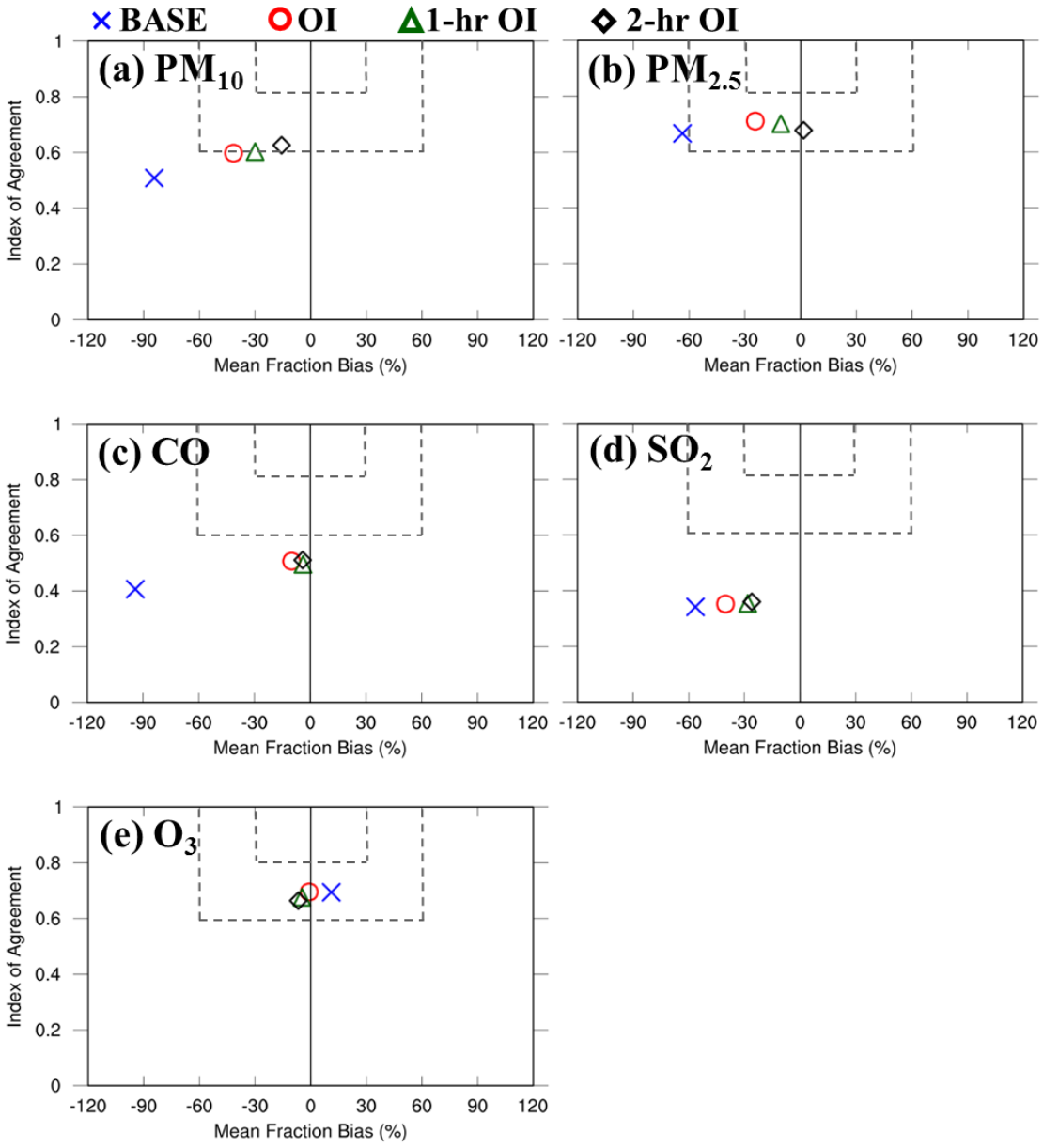

938

939 **Figure 13.** Soccer plot analyses for (a) PM_{10}, (b) $PM_{2.5}$, (c) CO, (d) SO_2, and (e) O_3. The
940 CMAQ-predicted concentrations were compared with the Air Korea observations. Blue crosses,
941 red circles, dark-green triangles, and black diamonds represent the performances calculated
942 from the BASE RUN, the DA RUNs with the OI system, the 1-hour (hr) OI system, and the 2-
943 hr OI system, respectively.

Table 1. Statistical metrics from BASE RUN and DA RUN with Air Korea observations over the entire period of the KORUS-AQ campaign.

	PM_{10}		$PM_{2.5}$		CO		SO_2		O_3	
	BASE RUN	**DA RUN**	**BASE RUN**	**DA RUN**	**BASE RUN**	**DA RUN**	**BASE RUN**	**DA RUN**	**BASE RUN**	**DA RUN**
N	101852		65383		101764		101764		101836	
IOA	0.51	0.60	0.67	0.71	0.41	0.51	0.34	0.35	0.69	0.70
R	0.34	0.40	0.51	0.53	0.28	0.21	0.14	0.15	0.50	0.52
RMSE	40.8	34.87	19.2	17.83	0.31	0.19	0.0068	0.0066	0.020	0.02
MB	-27.2	-13.54	-9.9	-2.43	-0.27	-0.04	-0.0009	-0.0004	0.003	-0.0024
ME	30.1	24.20	15.3	13.48	0.27	0.15	0.004	0.0034	0.015	0.015
MNB	-50.0	-18.17	-30.1	5.32	-62.0	3.14	3.1	17.77	48.0	30.22
MNE	60.7	52.35	62.6	62.77	62.9	40.67	93.1	93.56	70.2	61.34
MFB	-84.3	-41.61	-63.6	-24.41	-94.1	-10.00	-56.4	-40.20	11.1	-0.82
MFE	91.1	62.32	81.6	60.01	94.9	39.49	91.4	82.91	40.7	40.64

Table 2. Statistical metrics from BASE RUN and DA RUN with Air Korea observations at 00:00 UTC when the DA was conducted during the KORUS-AQ campaign.

	PM_{10}		$PM_{2.5}$		CO		SO_2		O_3	
	BASE RUN	**DA RUN**	**BASE RUN**	**DA RUN**	**BASE RUN**	**DA RUN**	**BASE RUN**	**DA RUN**	**BASE RUN**	**DA RUN**
N	1057		695		1024		1007		1043	
IOA	0.48	0.86	0.63	0.74	0.41	0.62	0.36	0.44	0.45	0.75
R	0.30	0.75	0.46	0.59	0.28	0.43	0.097	0.27	0.09	0.61
RMSE	47.2	23.92	21.5	18.21	0.35	0.16	0.0061	0.0039	0.023	0.012
MB	-32.2	-5.46	-11.5	2.80	-0.31	-0.01	-0.0019	-0.0009	0.015	0.002
ME	34.5	16.03	17.2	13.25	0.31	0.12	0.0039	0.0023	0.018	0.009
MNB	-54.9	-0.53	-33.2	26.17	-64.3	9.69	-20.1	7.35	100.4	27.45
MNE	64.0	36.07	63.1	59.77	64.8	30.69	86.7	55.27	107.8	43.81
MFB	-92.8	-13.38	-67.3	0.56	-98.7	1.81	-75.9	-17.39	43.7	12.16
MFE	98.8	38.41	84.3	48.30	99.1	27.14	99.9	56.23	52.9	31.53